Co-funded by the

MIND

Microbiology In Nuclear waste Disposal

(GRANT AGREEMENT: 661880)

DELIVERABLE D1.5

Microscopy and element mapping characterization studies of radionuclide microbe organic interactions

Editors: Mohamed L. Merroun (UGR)
Miguel A. Ruiz-Fresneda (UGR)

Date of issue of this report: 15.06.2018

Report number of pages: 33

Start date of project: 01/06/2015
Duration: 48 Months

This project has received funding from the Euratom research and training programme 2014-2018 under Grant Agreement no. 661880		
Dissemination Level		
PU	Public	
PP	Restricted to other programme participants (including the Commission)	
RE	Restricted to a group specified by the partners of the MIND project	
CO	Confidential, only for partners of the MIND project	**CO**

Publishable Summary

Deep geological repository (DGR) has been proposed as the safest option for the disposal of radioactive wastes. In this multi-barrier´s system, the radioactive wastes will be encapsulated by metal containers surrounded by artificial and natural barriers. Bentonite clay formations have been selected as reference materials for safety barriers in a DGR. In Spain, bentonite formations located in Cabo de Gata Natural Park (Almeria) were selected for this purpose. Microbes can affect the safety and performance of future DGRs at 3 different levels by: i) transformation of clay minerals through Fe(III) reduction; ii) corrosion of metal canisters; and iii) alteration of radionuclide mobility through different interaction processes. For instance, microorganisms are able to interact with typical elements of radioactive waste like selenium (Se), uranium (U) or curium (Cm) through different processes like biomineralization, biosorption or reduction leading to their mobilization or immobilization.

The main objectives of this study is to determine the role of *Stenotorphomonas bentonitica*, bacterial strain isolated from Spanish bentonites on the mobility and migration of radionuclides (Se(IV), Se(VI) and Eu(III)) under DGR relevant conditions using a multidisciplinary approach combining microscopy, spectroscopy, cell biology, radiochemistry, microbiology, etc. Selenium is a common component of radioactive waste and Eu(III) was considered as inactive analogue of trivalent actinides, Cm(III) and Am(III).

In the case of Se, this strain was able to reduce Se(VI) and Se(IV) to Se(0) forming Se nanostructures. Using a combination of number of microscopic techniques (STEM/HAADF, ESEM, FESEM, etc.), we could demonstrate here that *Stenotorphomonas bentonitica* reduce Se(IV) to Se(0) aerobically at pH7 , forming initially amorphous Se(0) (a-Se) nanospheres which subsequently transform to one-dimensional (1D) trigonal selenium (t-Se) nanostructures with diverse crystallinities, morphologies and sizes. Due to the low solubility of t-Se nanostructures compared to that of a-Se nanospheres and S(IV), the mobility of selenium in the environment may be significantly reduced. Time-dependent experiments showed that the cells of *S. bentonitica* and their proteins are involved into the transformation of amorphous Se(0) nanospheres (a-Se) to one-dimensional (1D) trigonal selenium (t-Se) nanostructures (hexagons, polygons and nanowires). In addition, *S. bentonitica* is also able to reduce Se(IV) under anaerobic and alkaline conditions (up to pH 10) producing a-Se nanospheres. However, the cells synthesize only intracellular Se(0) nanowires when this strain grow aerobically in presence of Se(VI).

The production of different volatile methylated Se species produced by *S. bentonitica* confirmed the change in the chemical speciation from Se(VI) and Se(IV) to Se(-II).

On the other hand, *S. bentonitica* is able to interact with Eu(III) mainly by a biosorption process under both aerobic and anaerobic conditions.

The Se reduction and production of crystalline *t*-Se nanostructures would be of great significance within the DGR system since the mobility of Se through the surrounding environment may be reduced. The biosorption of Eu(III), as a non-radioactive analogous to An(III) characteristics of nuclear waste, would also be of importance within the DGR system due to its retention through the surrounding environment.

Contents

1 Introduction

The influence of microbial processes onto the long-term performance of radioactive waste geological disposal it is nowadays an important issue considered for the safety assessment of this kind of disposal. The occurrence of microbial communities of the selected bentonite engineered barriers for the deep geological repository (DGR) system of radioactive wastes have been previously reported (1). In addition, during the construction operations of a repository, microorganisms could be accidentally introduced (2). The microbes could affect the long-term safety of the future DGRs at different levels. The clay-microbe interaction can produce clay mineral alterations that in turn affect the safety of this kind of disposal. The microbial communities may also affect the metal corrosion of the containers where the radioactive waste will be encapsulated by production of gases (CH_4, H_2, CO_2, etc.). Finally, microbes could be involved in the mobilization of radionuclides such as selenium (Se), uranium (U) or curium (Cm) through different interaction mechanisms (3–5). Selenium and uranium are common components of radioactive wastes produced by nuclear industry (6), while europium is an inactive analogue for trivalent actinides (e.g. Cm(III) and Am(III)) also present in nuclear wastes).

One of the objectives of WP1 consists of studying the interaction between bacterial isolates from bentonite clay formations and typical elements of radioactive wastes. Specifically, the University of Granada (UGR) are focused on Se and Eu interactions with the bacterial species *Stenotrophomonas bentonitica*, isolated from Spanish bentonites collected from Cabo de Gata Nature Park (Almería, Spain). For this purpose, a multidisciplinary approach combining microbiological, microscopic (STEM/HAADF, VPSEM, FEG-ESEM, etc.) and spectroscopic (XRD, ATR-IR, etc.) techniques were employed. This strain has been recently described as a new species and his whole genome have been sequenced (7). Carbon sources utilization and several physiological and biochemical characteristics were determined.

S. bentonitica is able to reduce selenate and selenite (Se^{VI} and Se^{IV}) aerobically to less toxic forms (Se^0 and Se^{-II}) producing crystalline nanostructures and Se volatile species. We have also reported the reduction of Se^{IV} to Se^0 under anaerobic and alkaline conditions relevant for the DGR system by this strain. The speciation of selenium determines its transport and migration behaviour in the environment affecting the safety of the planned repositories. On the other hand, *S. bentonitica* is also able to interact with Eu(III) mainly by a biosorption process under both aerobic and anaerobic conditions as indicated by STEM/HAADF and kinetic studies.

The results obtained by the UGR within the MIND project provide new insights into the impact of microbial processes in the speciation and mobilization of radionuclides in future radioactive repositories.

The MIND-project has received funding from the European Union's Euratom research and training program (Horizon 2020) under grant agreement 661880.

2 The interaction of bacterial isolate *Stenotrophomonas bentonitica* from Spanish bentonites with selenium

2.1 Experimental

Bacterial strain and growth conditions

The bacterial strain used in the present work was recently described by our Research Group as a novel species named *S. bentonitica* BII-R7^T (8). This strain was isolated from Spanish bentonites collected from the Cabo de Gata Nature Park (Almeria, Spain) (9). The cells were grown aerobically in Luria-Bertani (LB) broth medium (tryptone 10 g/l, yeast extract 5 g/l and NaCl 10 g/l, pH 7.0 ± 0.2) at 28 ºC and 180 rpm on a rotary shaker.

For anaerobic experiments, the cells were grown in modified R2A medium (peptone 0.5 g/l, glucose 0.5 g/l, potassium phosphate dibasic 0.3 g/l, magnesium sulphate 0.05 g/l) with added 10 mM sodium acetate and 20 mM sodium nitrate as electron donor and acceptor respectively. The solution was degassed with N_2 before being inoculated and incubated at a range of different pH values (from pH 7 to 11) at 28 ºC. The pH was adjusted by addition of acid (HCl) or base (NaOH).

Metal solution preparation

Sodium selenite (Na_2SeO_3) (Sigma-Aldrich) was prepared as a 1M stock solution by dissolving appropriate quantities in distilled water. Finally, the solution was sterilized by filtration using 0.22-μm syringe filters (Sartorius®).

Effect of selenite on the bacterial growth

The potential of *S. bentonitica* to tolerate selenite was assayed by growing the cells aerobically in LB liquid medium (30 ml) supplemented with 2 mM of Na_2SeO_3. Untreated (control) and Se^{IV}-treated cells were incubated at 28 ºC by shaking at 180 rpm. In addition, dead cells obtained by heating the biomass at 90 ºC and LB broth containing Se^{IV} (abiotic) were used as controls. Growth was evaluated by quantifying the total protein content in bacterial cell extracts using a modification of the method of Dhanjal and Cameotra, 2010 (10).

The minimal inhibitory concentrations (MICs) of Se^{IV} were determined in triplicates. Cells of the isolate were grown to late exponential phase to a final optical density (O.D) of 0.9 (at 600 nm) in LB broth and washed twice with 0.9% NaCl. Finally, 10 μl of the cell suspension was inoculated to LB agar supplemented with increasing concentrations of Se^{IV} from 1 to 400 mM. Afterwards, the plates were incubated at 28 ºC for 48 h. The MIC was defined as the lowest concentration of the element at which complete inhibition of colony formation is observed (11).

Flow cytometry

The cell viability and the metabolic activity of *S. bentonitica* in the presence of Se^{IV} under oxic conditions were determined by using flow cytometry technique. For this purpose, the

The MIND-project has received funding from the European Union's Euratom research and training program (Horizon 2020) under grant agreement 661880.

bacterial strain BII-R7 was amended with 2 mM of Se^{IV} and incubated at 28 ºC and 180 rpm on a rotary shaker. All experiments were done in triplicates. After 24 and 144 h of incubation, the cells were collected by centrifugation at 11000 rpm at 4°C for 10 min. The resultant pellet was washed four times in phosphate buffered saline (PBS) pH 7. Then, the cells were dissolved in PBS adjusting the cellular density to approximately 10^6 cells/ml. For cell viability test, fluorescein diacetate (FDA) and propidium iodide (PI) were added into each sample to a final concentration of 20 µl/ml and 2µl/ml respectively. For metabolic activity test, 3,30-dihexyloxacarbocyanine iodide (DiOC6) was employed to a final concentration of 20µl/ml. Finally, the samples were analysed by Forward Scatter using a FACSCantoII™ cytometer (Becton Dickinson) available at the "Centro de Instrumentación Cientifica" of the University of Granada. Dead cell controls were obtained by heating the biomass at 90 ºC.

These experiments were also assayed anaerobically in cultures amended with Se^{IV} ranging from 0.1 to 2 mM after 12 and 60 h of incubation.

Microscopic analysis

The morphology, elemental composition analysis and cellular location of reduced Se were analysed by using **Scanning-Transmission Electron Microscopy (STEM)** equipped with energy dispersive X-ray (EDX). EDX analysis was performed at 300 kV using a spot size of 4 Å and a live counting time of 50 s. The structural characterization of Se nanostructures was performed by using selected-area electron diffraction (SAED) and high-resolution TEM combined with Fast Fourier Transform (FFT).

STEM samples were prepared as described in Merroun *et al.* 2005 (12) after 24, 48, 72 and 144 h of incubation for aerobic Se^{IV}-amended cultures at neutral pH. For anaerobic and alkaline (pH 10) cultures supplemented with Se^{IV} the samples were prepared after 120 h under the same Se^{IV} stress (2 mM). In the case of Se^{VI}-amended cultures samples were prepared after 24 h to a final concentration of 200 mM. Finally, the samples were examined under High-Angle Annular Dark Field Scanning Transmission Electron Microscope (HAADF-STEM) FEI TITAN G2 80-300. STEM specimen holders were cleaned by plasma prior to STEM analysis to minimize contamination.

Variable Pressure Field Emission Scanning Electron Microscopy (VP-FESEM) equipped with an X-ray detector Raman spectroscopy system enabled an in situ 3-D structural and elemental characterization of the SeNPs produced by the cells. Cell suspensions amended with 2 mM Se^{IV} after different incubation times and conditions (aerobically, anaerobically and alkaline conditions) and 200 mM Se^{VI} (after 24 h and oxic conditions) were fixed in 3% glutaraldehyde in 0.05 M sodium cacodylate buffer (pH 7.2) for 24 h at 4 ºC. Afterwards, the samples were washed three times with the same buffer. The resultant pellets were fixed in 1% osmium tetroxide solution (OsO_4) in cacodylate buffer before dehydration in a graded ethanol solutions in water. The critical point drying method was also used to dehydrate the samples. Finally, they were coated with carbon and stored in a desiccator. The samples were analysed under Variable Pressure Field Emission Scanning Electron Microscope Zeiss SUPRA 40VP.

Field Emission Gun Environmental Scanning Electron Microscopy (FEG-ESEM) equipped with secondary and circular backscatter electron detectors (ETD and CBS) enabled to determine the presence of organic matter surrounding the biogenic SeNPs. This technique

The MIND-project has received funding from the European Union's Euratom research and training program (Horizon 2020) under grant agreement 661880.

was also applied to explain the biotransformation of *a*-Se nanospheres to *t*-Se nanostructures. Thus, the cells where contacted for 24 h with solutions containing two different types of *a*-Se nanospheres: 1) Chemically (CheSeNPs); and 2) organically produced SeNPs (OrgSeNPs). Chemical SeNPs were produced by reduction of sodium selenite (5 mM) by reduced glutathione (GSH) (20 mM) at 28 ºC. The OrgSeNPs were synthesized using proteins (Bovine Serum Albumin; BSA) (0.01 g/l) in addition to GSH (20 mM) and Se^{IV} (2 mM). Finally, the samples were analysed under FEG-SEM Microscope FEI QEMSCAN 650F.

X-ray diffraction

XRD analysis was carried out to determine the size and crystalline phase of biogenic Se nanoparticles. *S. bentonitica* cells treated aerobically with 2 mM of Se^{IV} for 144 h were centrifuged at 10000 rpm for 10 min. The resultant pellet was washed with double distilled water. The washed samples were dried at 28 ºC for 24 h. X-ray patterns of the biogenic SeNPs were obtained with a Bruker D8 Advanced diffractometer associated to a LINXEYE detector available at the University of Granada. The obtained diffractograms were analysed using the software DIFFRAC PLUS.

Detection and identification of volatile Se compounds produced by S. bentonitica.

A combined thermal desorption GC-MS (Gas Chromatography – Mass Spectrometry) system were employed for the detection and identification of selenium volatile species produced by the bacterial strain *S. bentonitica*. Cultures of *S. bentonitica* were grown in the presence of Se^{IV} (0.1 and 2 mM) into 250 ml conical Quickfit® flask capped with Suba-Seals (Sigma®) to avoid the loss of gases during gas extraction with hypodermic syringes. Se^{IV}-free cultures (biotic) and Se^{IV}-amended media (abiotic) were used as controls. The gaseous samples were taken and analysed as described previously by Eswayah *et al*. 2007 (13) after 24 and 144 h of incubation. The National Institute of Standards and Technology (NIST) MS search program (version 2011) was employed to identify compounds based on their mass spectrum.

2.2 Se^{IV} bioreduction

2.2.1 Aerobic conditions

Se^{IV} reduction and effect Se^{IV} on the bacterial growth.

The ability of *S. bentonitica* to reduce aerobically Se^{IV} to Se^{0} was tested in LB liquid medium at 2 mM selenite. Se^{IV}-treated cultures of *S. bentonitica* turned into an intense red colour after 24 h incubation, in contrast to untreated cultures (blanks) (**Figure 1**). This colour change reveals the capacity of the strain to reduce Se^{IV} to Se^{0} (14). The Se^{IV} reduction is mediated by a biological rather than chemical process since no colour change were observed in abiotic and dead cells control samples supplemented with Se^{IV}. MIC of Se^{IV} for the growth

The MIND-project has received funding from the European Union's Euratom research and training program (Horizon 2020) under grant agreement 661880.

of the studied strain in solid media was 400 mM as red precipitates and cell growth were observed in all assayed Se^{IV} concentrations ranged from 1 to 200 mM (data not shown).

Figure 1. Cultures of Stenotrophomonas bentonitica in LB broth liquid medium without (A) or with 2 mM Se^{IV} (B) after 24 h showing the reduction of Se^{IV} to Se^{0} as indicated by the produced red precipitate.

The growth profile of the cells under Se^{IV} stress was studied and expressed as total protein content as function of time. In comparison to controls (0 mM Se^{IV}), the microbial growth was negatively affected in presence of Se^{IV} (from 0.1 to 4 mM) (**Figure 2**). It is important to note that growth of *S. bentonitica* cells presented longer lag phase of about 48 hours in the presence of Se^{IV}. This suggests an adaptation of the cells to Se^{IV} stress. The lag phase observed in the present and other studies (15) could be probably associated with a differential expression of enzymes involved in the Se^{IV} tolerance. Whole genome analysis of *S. bentonitica* revealed the presence of genes codifying enzymes described for their ability to reduce Se^{IV} to Se^{0} (7). Glutathione reductase and thioredoxin reductase as well as NADH-dependent enzymes such as NADH: flavin oxidoreductase (OYE family) previously reported to be implicated in the reduction of this oxy-anion (16), have been identified in the genome of *S. bentonitica*. Several mechanisms have been proposed for the reduction of selenite in microorganisms including Painter-type reaction (17), thioredoxin reductase system (18), sulphide mediated reduction (19), dissimilatory reduction (20), etc.

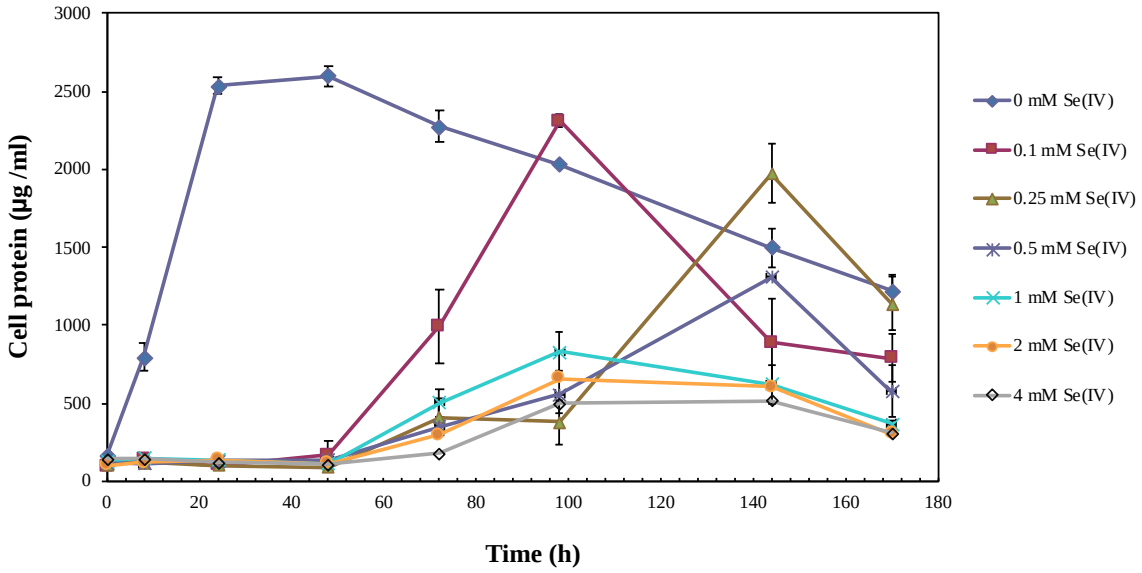

Figure 2. Effects of different selenite concentrations (0, 0.1, 0.25, 0.5, 1, 2, and 4 mM) on the growth of the bacterial strain Stenotrophomonas bentonitica. Selenite was added at time zero. Each curve shows means based on the results of three experiments.

The MIND-project has received funding from the European Union's Euratom research and training program (Horizon 2020) under grant agreement 661880.

The effect of Se^{IV} on cell viability of *S. bentonitica* was studied by the live-dead staining approach conducted with propidium iodide (PI) and fluorescein diacetate (FDA). PI enters to cells with damaged membranes staining nucleic acids of dead cells (21), while FDA stains viable cells (22). With regard to the metabolic activity test, the fluorescent dye $DiOC_6$ was used in order to bind polarized membranes of active cells (23). The percentages of viable and active cells of *S. bentonitica* population untreated and treated with an initial Se^{IV}) concentration of 2 mM during 24 and 144 h are displayed in **Figure 3**. Cell viability was affected negatively by selenite. Specifically, 46.3 and 36.4 % of cell populations were found to be viable after 24 and 144 h time incubation, respectively. In contrast, higher amount of viable cell population (100 %) was observed in untreated samples. On the other hand, the metabolic activity test showed a lower oxidative response under Se^{IV} stress. Specifically, 59 and 72.2 % were found to be active after 24 and 144 h respectively, comparing with untreated cells (97 and 97.8 % of active cells). This increase on cell activity from 59 to 72.2 % could be explained by the fact that at 24 h cells are still in the lag phase (see Fig. 2), probably adapting their metabolism to respond to selenium stress. Once they are able to tolerate selenium they grow as observed at 144 h. The results of the flow cytometry concur with the growth curve suggesting a toxic effect of Se^{IV} on *S. bentonitica* cells.

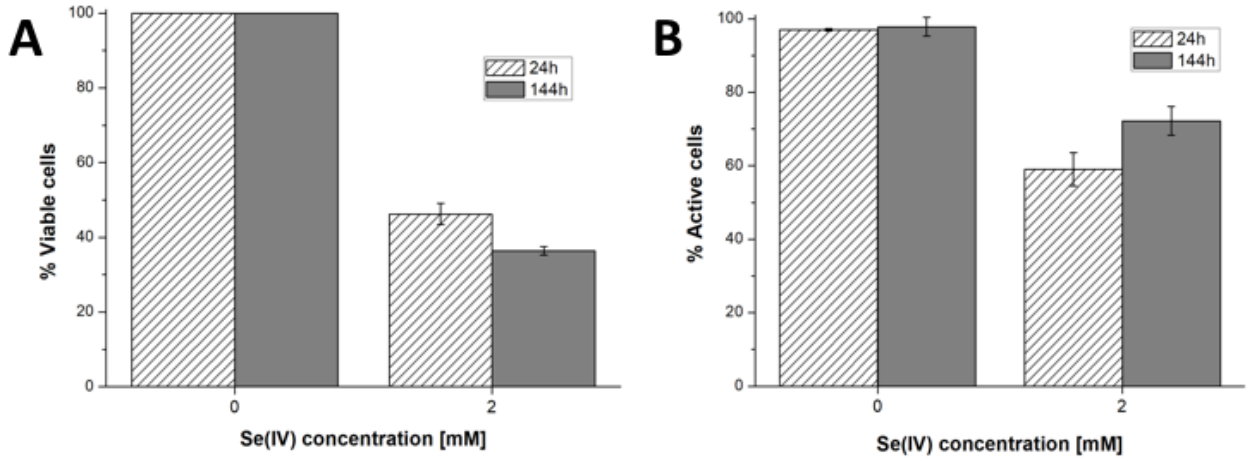

Figure 3. Percentage of viable (A) and active cells (B) of S. bentonitica under different selenite concentrations (0 and 2 mM) and contact times (24 and 144h) aerobically.

Structural characterization of Se reduction products.

STEM micrographs and Energy dispersive X-ray (EDX) analysis revealed the presence of extracellular Se nanostructures when cells were grown on Se^{IV} at 2 mM for 144 h (**Figure 4**). In addition, very few intracellular SeNPs were observed. The presence of intracellular and extracellular SeNPs suggested their intracellular formation before their release into the extracellular space in response to selenite stress.

The Se nanostructures identified by STEM exhibited different shapes: spheres, nanowires, hexagons, polygons, etc. Energy dispersive X-ray (EDX) elemental mapping derived from these accumulations showed that they are mainly composed of Se, in addition to S (**Figure 4**).

The MIND-project has received funding from the European Union's Euratom research and training program (Horizon 2020) under grant agreement 661880.

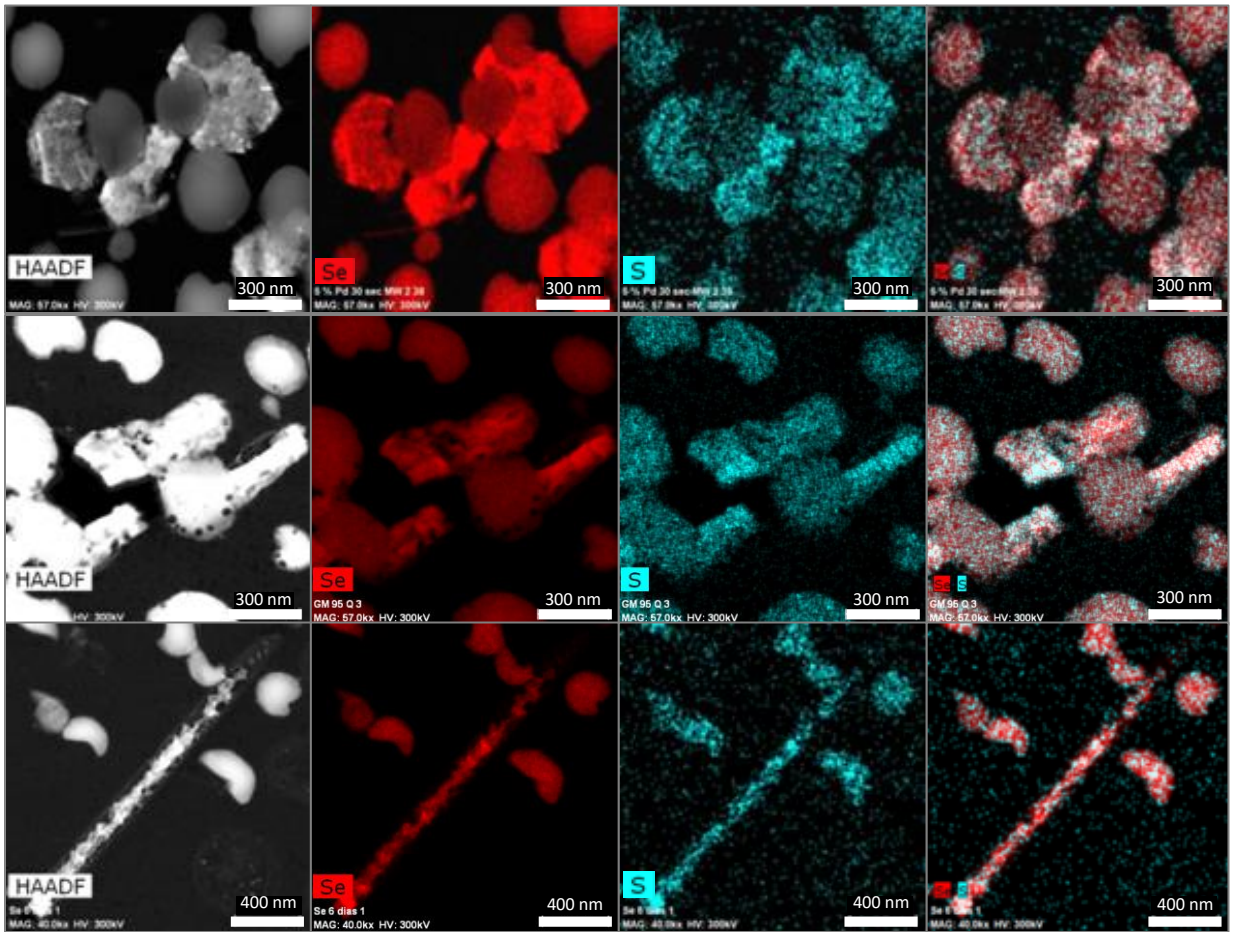

Figure 4. HAADF-STEM micrographs of thin section showing the different morphologies (spherical, hexagonal, polygonal, and nanowires) of SeNPs produced by S. bentonitica after 144 h of incubation. EDX element-distribution maps confirmed that they are mainly composed of Se and S (Ruiz-Fresneda et al. 2018 (in press)) (24).

Extensive accumulations of Se nanospheres with two considerable different sizes were detected. Specifically, smaller nanospheres with diameters of 20 to 30 nm and bigger NPs around 200 nm were found (**Figure 5**). EDX microanalysis indicated that they are mainly composed of Se and S (**Figure 5**). In addition, selected area electron diffraction (SAED) pattern of nanospheres indicated their amorphous nature (**Figure 6A-B**). To a lesser extent, hexagonal-shaped nanostructures from 100 to 400 nm in size were produced (**Figure 6C**). The HRTEM image from an individual hexagonal-shaped nanoparticle showed 2 distinct lattice spacings of 0.37 and 0.29 nm corresponding to (100) and (101) planes of *t*-Se, respectively **(Figure 6D and 6E).** The SAED pattern indicated that hexagonal-shaped nanostructures can be well indexed to *t*-Se (**Figure 6F**). In addition, the lattice spacing values obtained for all the diffraction rings from the FFT of the image (**Figure 6G**) are in agreement with the trigonal phase of Se. The last type of SeNP shape detected consisted of nanowires around 30 nm in diameter (**Figure 6H**). The HRTEM image from an individual nanowire showed 2 distinct lattice spacings of 0.37 and 0.19 nm corresponding to (100) and (111) planes of *t*-Se **(Figure 6I and 6J)**. The SAED spots revealed that Se nanowires are polycrystalline (**Figure 6K**). In addition, the FFT of the image shown in **Figure 6L** further confirms the trigonal phase of selenium.

The MIND-project has received funding from the European Union's Euratom research and training program (Horizon 2020) under grant agreement 661880.

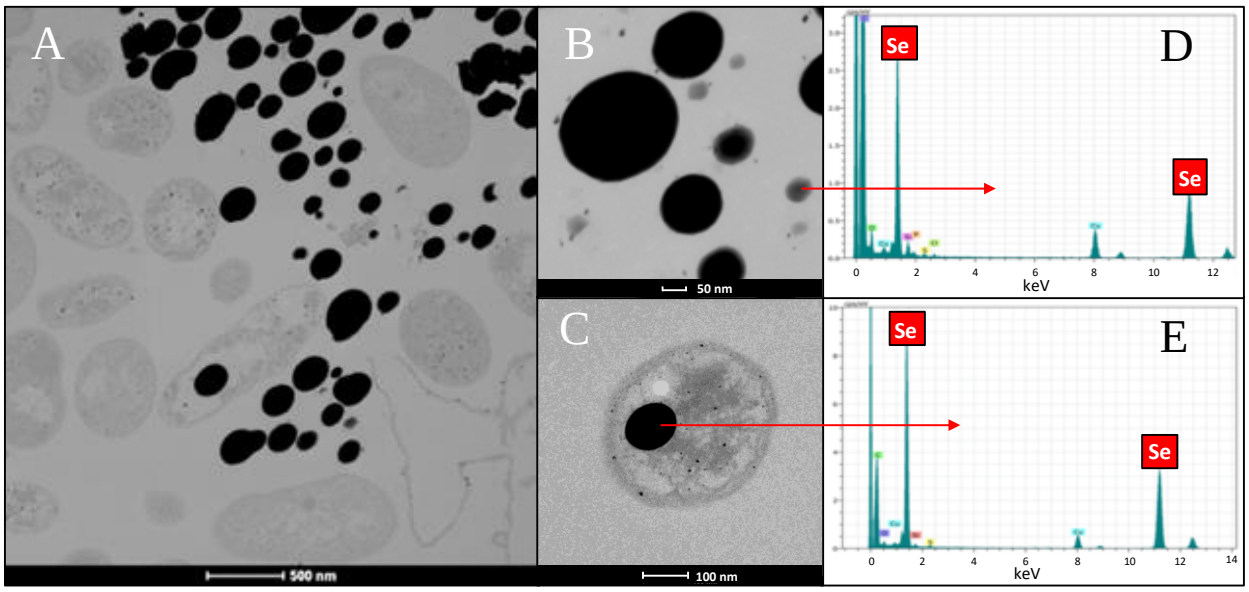

Figure 5. HAADF-STEM micrographs of thin section showing extracellular and intracellular SeNPs with two different sizes produced by the cells of Stenotrophomonas bentonitica (A, B and C). Scale bars: 500 nm (A), 50 nm (B) and 100 nm (C). EDX analysis image of a single SeNP (D and E) (Ruiz-Fresneda et al. 2018 (in press)) (24).

These results match very well with XRD diffraction pattern obtained from the same sample. The XRD peaks obtained showed the main peaks characteristic for crystalline *t*-Se (COD-9008579) at 2Θ values of 23.5°, 29.7°, 41.4°, 43.7° and 45.4° (**Figure 7**) corresponding to the crystal planes (100), (101), (110), (102) and (111), respectively. The Raman spectrum derived from Se aggregations also supports the formation of *t*-Se nanostructures by the appearance of peaks at 232 and 235 cm^{-1} (**Figure 8**). The distinctive Raman peak corresponding to the symmetric stretching mode of *t*-Se is located at 235 cm^{-1}, which can be attributed to the vibration of Se helical chains (25).

The MIND-project has received funding from the European Union's Euratom research and training program (Horizon 2020) under grant agreement 661880.

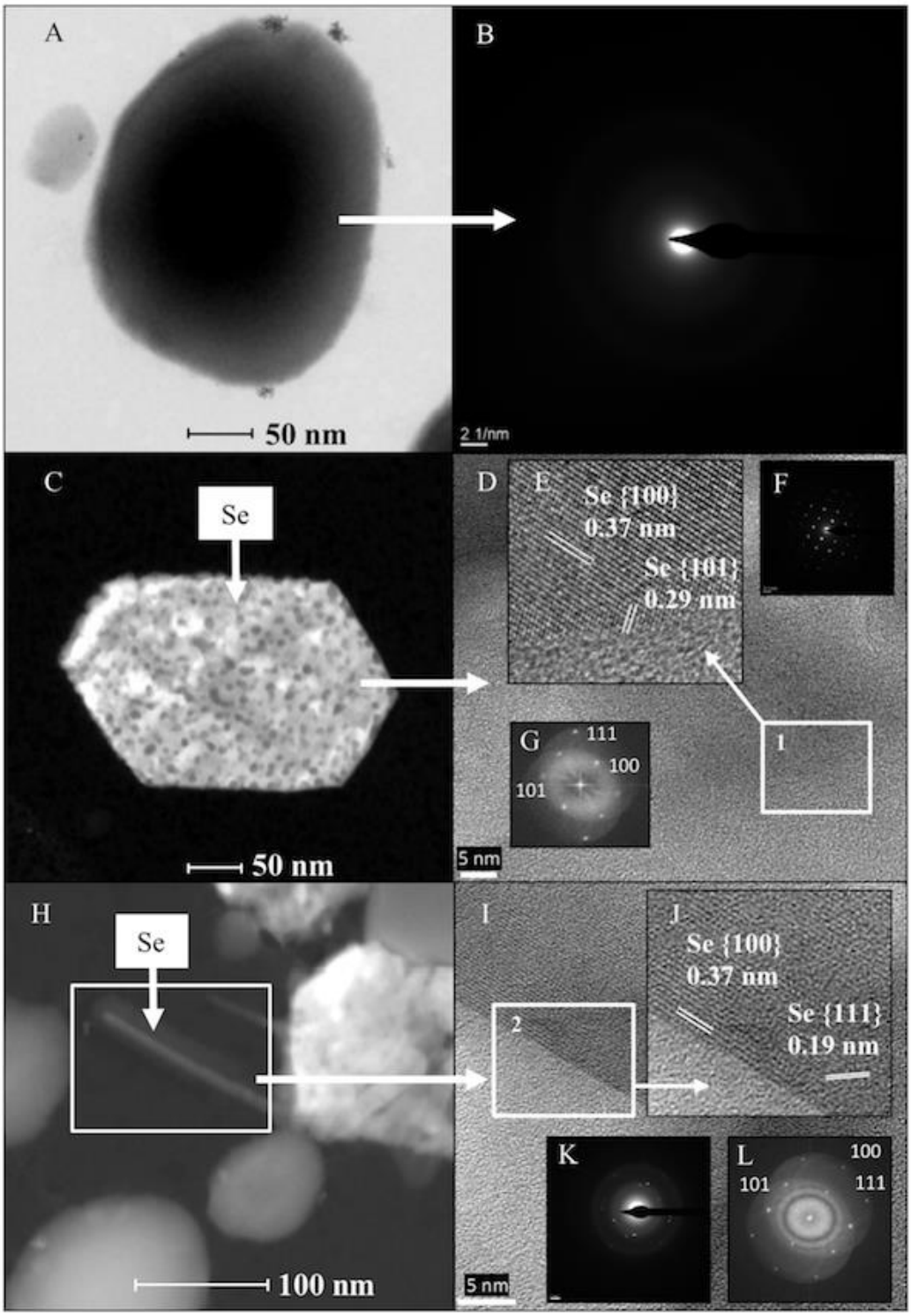

Figure 6. HAADF-STEM micrograph (A) and SAED pattern (B) of a single spherical SeNP. HAADF-STEM micrograph (C) and HRTEM image (D) of a single hexagonal-shaped SeNP. Panel E is the magnification from HRTEM image corresponding to the area 1. SAED pattern (F) and FFT (G) corresponding to the HRTEM of the single hexagonal-shaped SeNPs. HAADF-STEM micrograph (H) and HRTEM image (I) of a single selenium nanowire. Panel J is the magnification from HRTEM image corresponding to the area 2. Panel K and L shows the SAED pattern and the FFT corresponding to the HRTEM of the single Se nanowire. Scale bars: 50 nm (A), 2 1/nm (B), 50 nm (C), 5 nm(D), 100 nm (H) and 5 nm (I) (Ruiz-Fresneda et al. 2018 (in press)) (24).

The MIND-project has received funding from the European Union's Euratom research and training program (Horizon 2020) under grant agreement 661880.

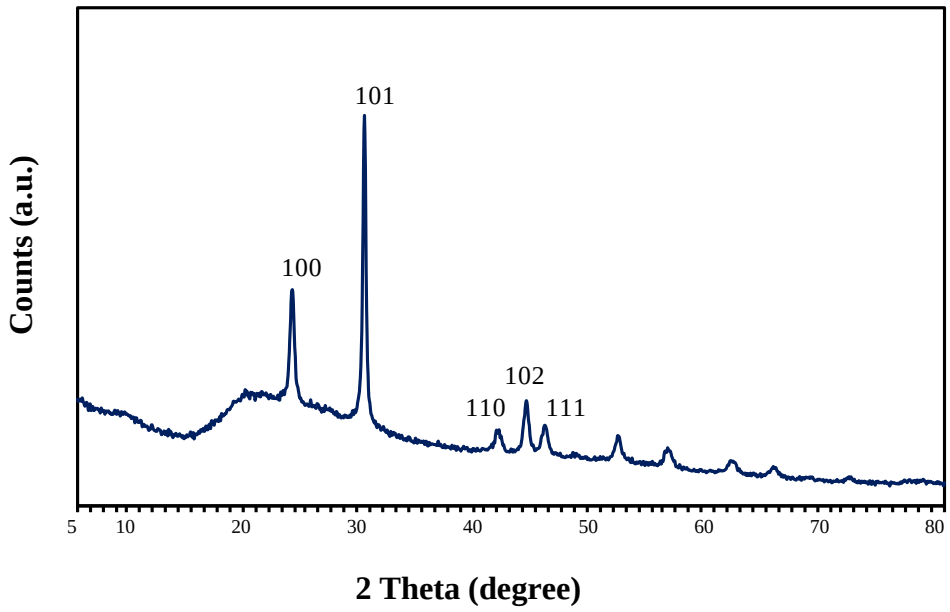

Figure 7. X-ray diffraction pattern of selenium nanoparticles synthesized by Stenotrophomonas bentonitica after 144 h incubation (Ruiz-Fresneda et al. 2018 (in press)) (24).

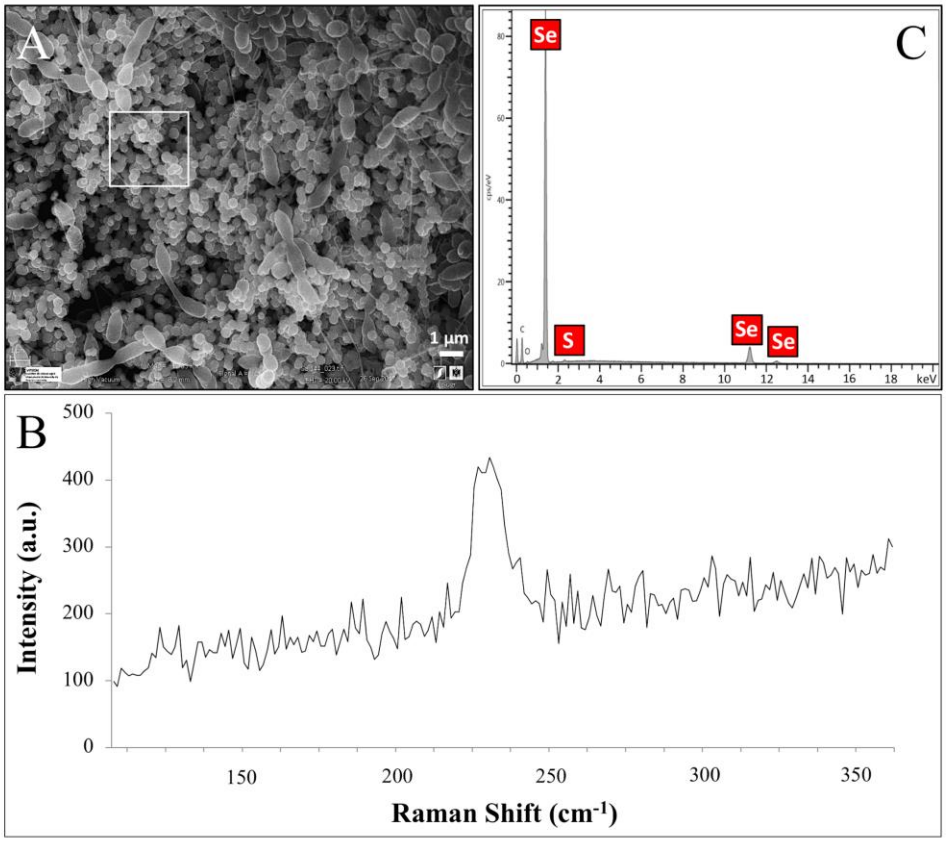

Figure 8. VPSEM micrographs (Scale bar: 1µm) of S. bentonitica surrounded by extensive accumulations of Se nanospheres (A) and their respective Raman spectrum (B). EDX analysis (selected area shown) indicated the presence of Se and S in the nanospheres (C) (Ruiz-Fresneda et al. 2018 (in press)) (24).

The MIND-project has received funding from the European Union's Euratom research and training program (Horizon 2020) under grant agreement 661880.

Biotransformation process from Se nanospheres to crystalline Se nanostructures

The production of different Se nanostructure shapes by the cells is a time dependent process. After incubation period of 24 h, 30-200 nm sized biogenic individual *a*-Se nanospheres were synthesized (**Figure 9A**). The latter start to coalesce forming aggregates after 48 and 72 h (**Figure 9B and 9C**). After 144 h the cells were able to produce a mixture of one-dimensional (1D) *t*-Se nanostructures with different shapes (*e.g*. nanowires, hexagons, polygons, etc.) and diameters, in addition to *a*-Se (**Figure 9D**). These results suggested the probable transformation of *a*-Se nanospheres to *t*-Se nanostructures with different shapes.

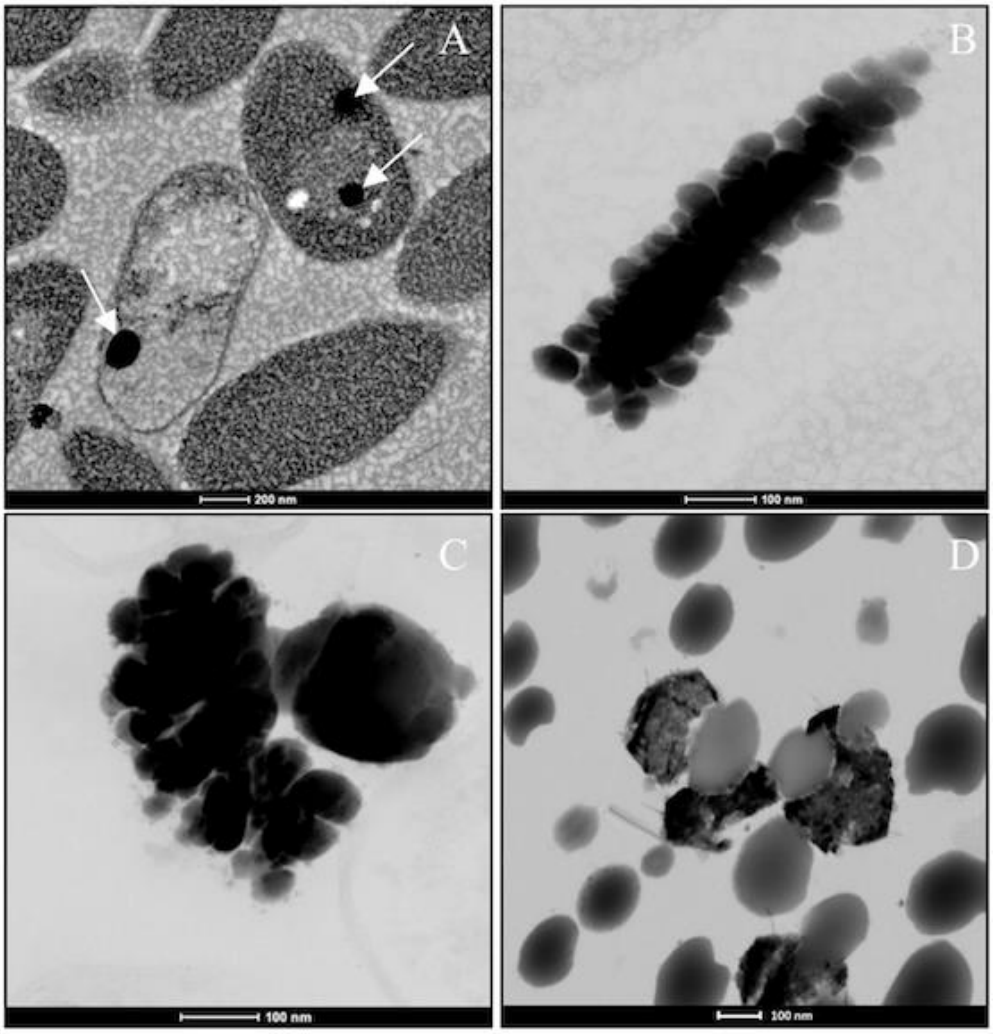

Figure 9. HAADF-STEM pictures showing individual a-Se nanospheres (white arrows) after 24 h (A) and forming aggregates after 48 h (B) and 72 h (C). Mixture of different t-Se nanostructures and a-Se nanospheres produced after 144 h (D). Scale bars: 200 nm (A), 100 nm (B-D) (Ruiz-Fresneda et al. 2018 (in press)) (24).

In order to determine the impact that bacterial cells and their components (e.g. proteins) can have on transformation of *a*-Se NPs to *t*-Se NPs we performed a series of control experiments where *S. bentonitica* cells were contacted for 24 h with chemical (CheSeNPs) and organically produced SeNPs (OrgSeNPs). The organic SeNPs were synthesized using proteins (*i.e.* BSA) as template and representing the early stage of biogenic formation of amorphous SeNPs.

The MIND-project has received funding from the European Union's Euratom research and training program (Horizon 2020) under grant agreement 661880.

When the experiment was conducted without the presence of bacteria, TEM images revealed the presence of only amorphous spherical SeNPs with homogenous size distribution in both CheSeNPs and OrgSeNPs samples (data not shown). In the presence of bacteria, CheSeNPs were distributed in the extracellular space without any contact with the cells (**Figure 10A**). However, both Se nanowires and nanospheres associated with cells were detected when proteins (BSA) and bacteria were present (**Figure 10B and 10C**). In the later sample, spherical SeNPs aggregates are formed by high number of individual Se nanospheres which seem to be embedded in an organic matrix. The aggregation seems to take place along an axis which could correspond to the flagella-like proteins structures characteristic of this bacterium (**Figure 10C**). This aggregation has been previously reported to be a crucial step during the transformation process to Se nanowires (26).

Biogenic Se nanospheres produced by *S. bentonitica* seem to be also surrounded by organic matrix and to aggregate along the flagella-like proteins (**Figure 10D**). These results suggest that organic matter (mainly proteins capping the NPs and flagella-like proteins) produced by *S. bentonitica* have an important role in the aggregation and hence in the transformation from nanospheres to nanowires.

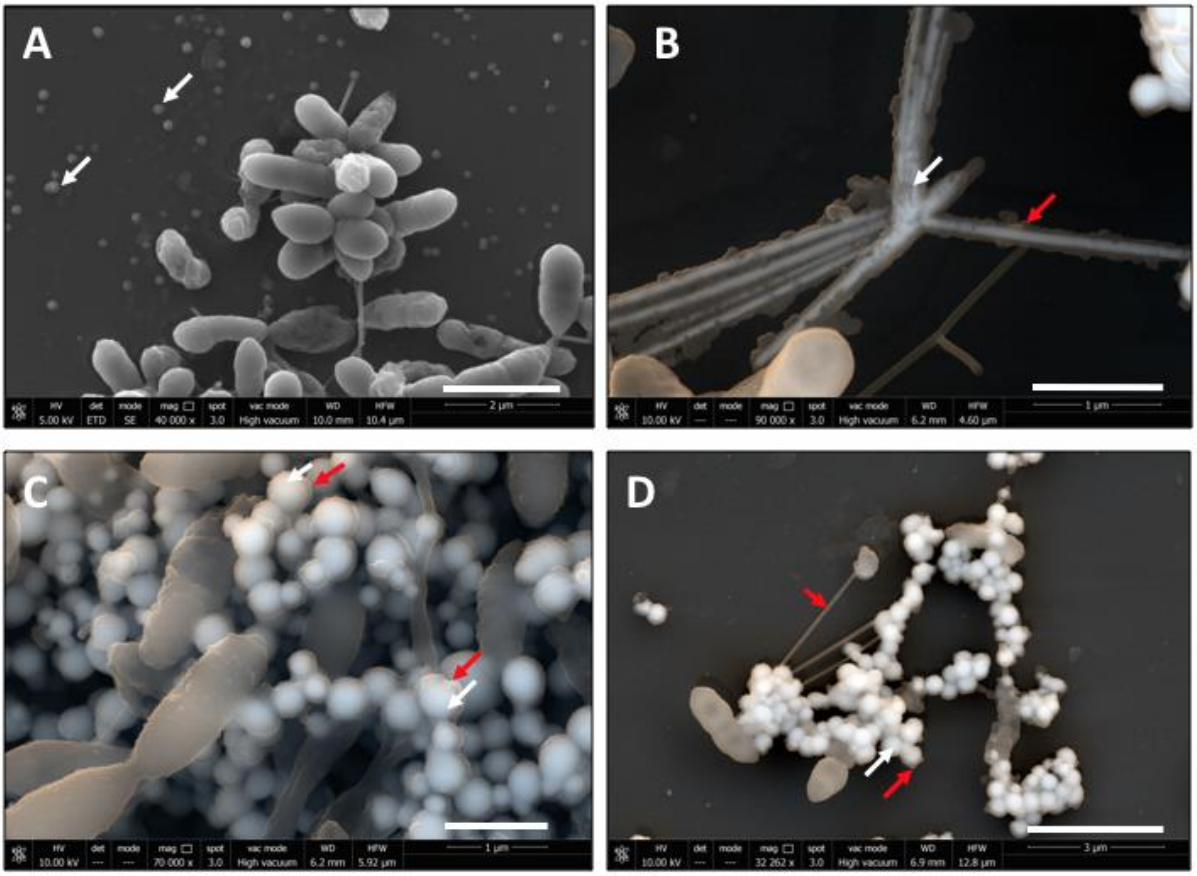

Figure 10. FEG-ESEM of CheSeNPs (white arrows) distributed within the extracellular space in the presence of S. bentonitica cells (A). Scale bar: 2 µm. Selenium nanowires (B) and nanospheres (white arrows) (C) surrounded by organic matter (red arrows) in S. bentonitica cultures treated with OrgSeNPs (with BSA). Scale bar: 1 µm. Se nanospheres aggregates produced by S. bentonitica surrounded by organic matter and flagella-like proteins (D). Scale bar: 3 µm (Ruiz-Fresneda et al. 2018 (in press)) (24).

The MIND-project has received funding from the European Union's Euratom research and training program (Horizon 2020) under grant agreement 661880.

We proposed that transformation to *t*-Se nanostructures occurs once the nanospheres have been released from the cells, probably through a process of cell lysis. This is supported by the appearance of some SeNPs in the proximity of lysed cells (data not shown). The transport of Se nanospheres across the membrane seems unlikely due to their large size and no detection of vesicles in HAADF-STEM analysis. A transformation process has been proposed where the released Se nanospheres from the intracellular space start to coalesce and probably growth on the axis of flagella-like proteins (**Figure 11**). Finally, they cristallyze forming the different *t*-Se nanostructures. However, more experimental data are needed to proof this proposed transformation mechanism model.

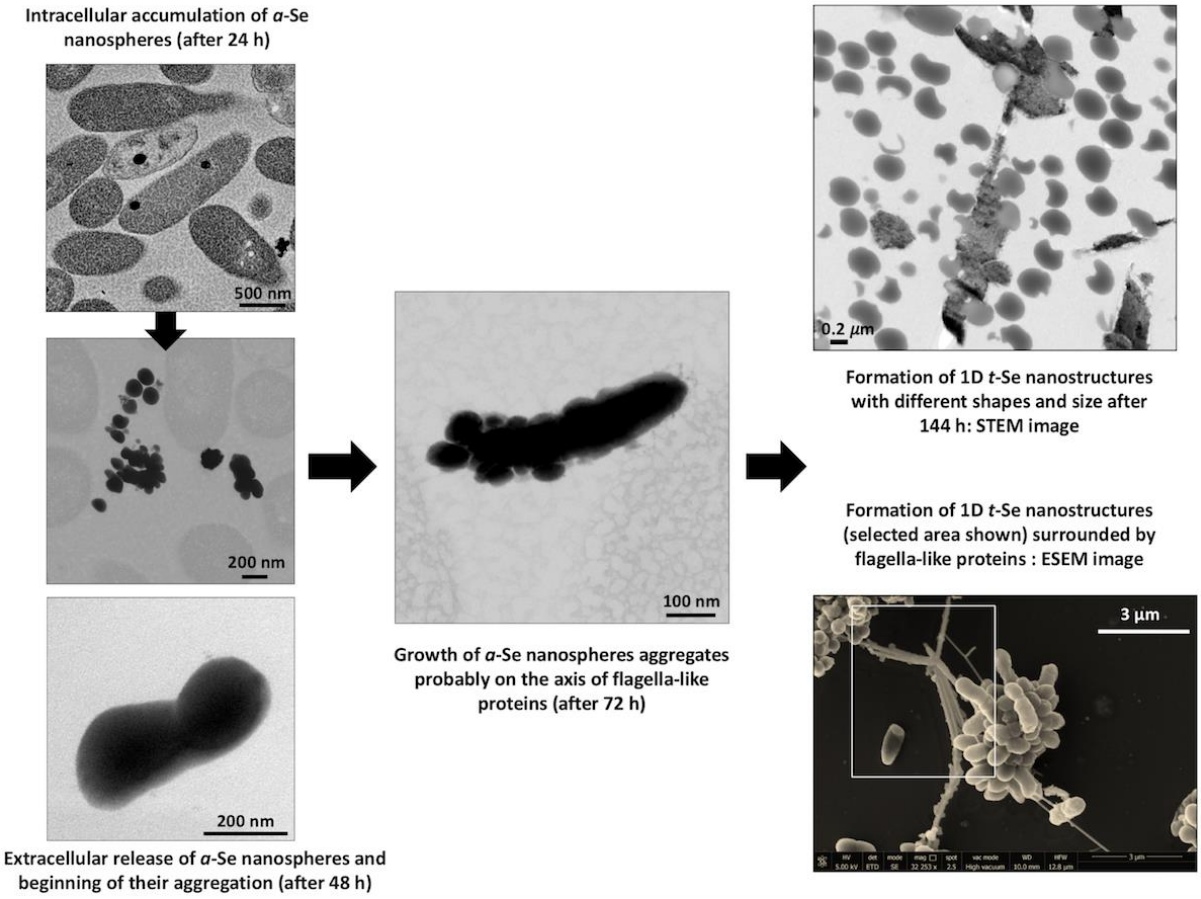

Figure 11. Proposed mechanism of time-dependent transformation of a-Se nanospheres to the different 1D t-Se nanostructures (Ruiz-Fresneda et al. 2018 (in press)) (24).

Detection and identification of volatile Se compounds produced by S. bentonitica.

The headspace gas above the cultures was sampled (200 ml) and analyzed by GC-MS system in order to identify the volatile selenium species. GC-MS extracted ion chromatograms for 80 m/z (specific for selenium) of the samples amended with 0.1 and 2 mM Se^{IV} concentration showed the production of dimethyl diselenide (DMDSe) and dimethyl selenenyl sulphide (DMDSeS) after 24 and 144 h (**Figure 12A and 12B**). No differences in the production of volatile Se species between different Se^{IV} initial concentration and incubation time employed were observed. The absence of Se volatile compounds in biotic and abiotic controls

The MIND-project has received funding from the European Union's Euratom research and training program (Horizon 2020) under grant agreement 661880.

suggested that they are produced by the bacterial cells (data not shown). It is important to note that dimethyl disulfide (DMDS) was detected in both samples and controls. This compound could be involved in the formation of selenium volatile species. Chasteen (1993) (27) previously reported that a disproportionation reaction between DMDSe and DMDS to produce DMSeS is quite probable. The detection of different volatile methylated Se species confirmed the change in the chemical speciation from Se^{IV} to Se^{-II}. These measurements were conducted in collaboration with Dr. Gardiner Philip from the Sheffield Hallam University.

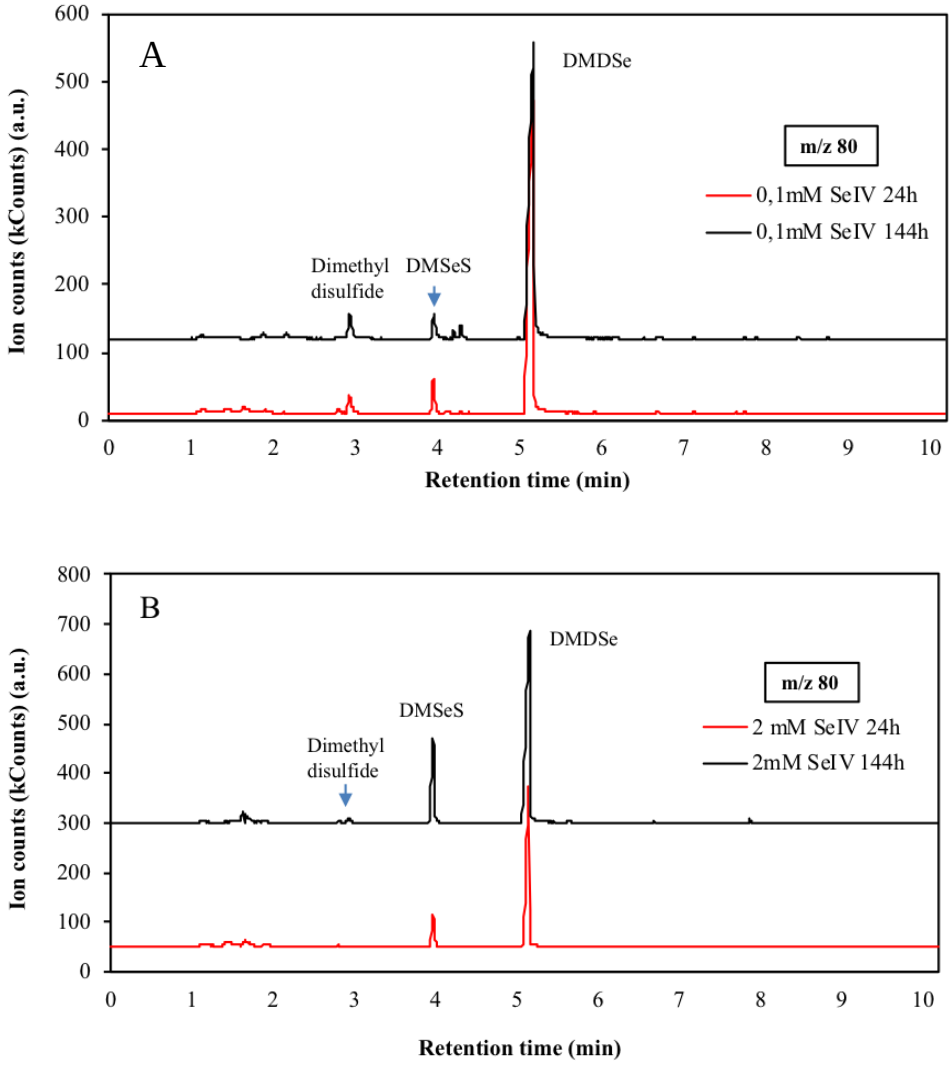

Figure 12. GC-MS chromatograms of the headspace gas of S. bentonitica cultures supplemented with 0.1 (A) and 2 mM of Se^{IV} (B) after 24 and 144 h obtained by selecting the 80 m/z ion specific for selenium.

2.2.2 Se^{IV} reduction at anaerobic and alkaline conditions

The strain *S. bentonitica* is also able to reduce Se^{IV} under anaerobic and alkaline conditions. Specifically the reduction occurs from neutral to pH 10 as indicated the red precipitation (**Figure 13**). At pH 11 there is no reduction since no red precipitates appeared. In the same

The MIND-project has received funding from the European Union's Euratom research and training program (Horizon 2020) under grant agreement 661880.

way that aerobic experiments, non-production of red precipitates in biotic and abiotic controls suggests that the reduction is conducted by the bacterial strain. Although the reduction occurs, the strain is not able to growth under these conditions (data not shown).

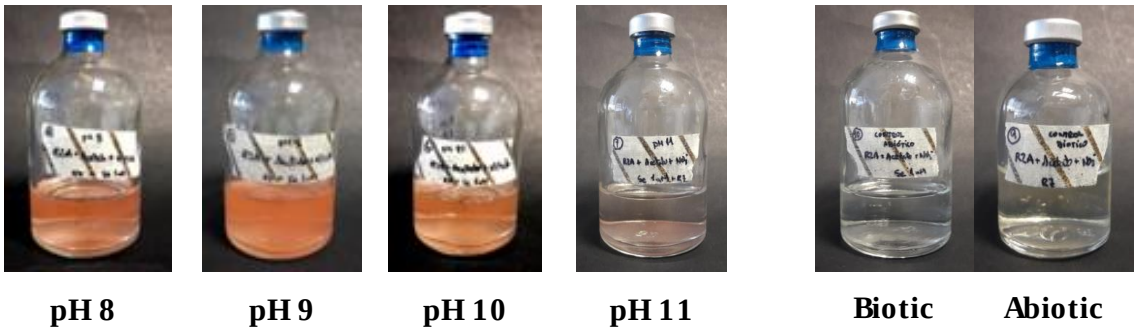

Figure 13. Cultures of S. bentonitica showing the reduction of Se^{IV} from pH 8 to 10 indicated by the production of red precipitates. No reduction occurs in cultures at pH 11 and in biotic (Se^{IV}- free cultures) and abiotic controls.

The effect of Se^{IV} on cell viability and activity under anaerobic conditions at neutral pH was studied by flow cytometry. A decrease on viability was observed in presence of 2 mM Se^{IV} comparing with lower concentrations (from 0.1 to 0.5 mM) at both incubation time (12 and 60 h) (**Figure 14A**). However the cell viability was found to be a little bit higher after 60 h than 12 h under 2 mM Se^{IV} stress. Regarding the cell activity, a decrease was observed in presence of 2 mM Se^{IV} comparing with lower concentrations (from 0.1 to 0.5 mM) at both incubation time (12 and 60 h) (**Figure 14B**). It could be appreciated that cell activity is higher after 60 h incubation than 12 h. This could be explained by the fact that at the first 12 h of incubation the cells are adapting to the new conditions (Se^{IV} stress) (see fig. 2). After 60 h the cells are at the beginning of the exponential phase and start to grow. As a consequence, their viability and activity are higher.

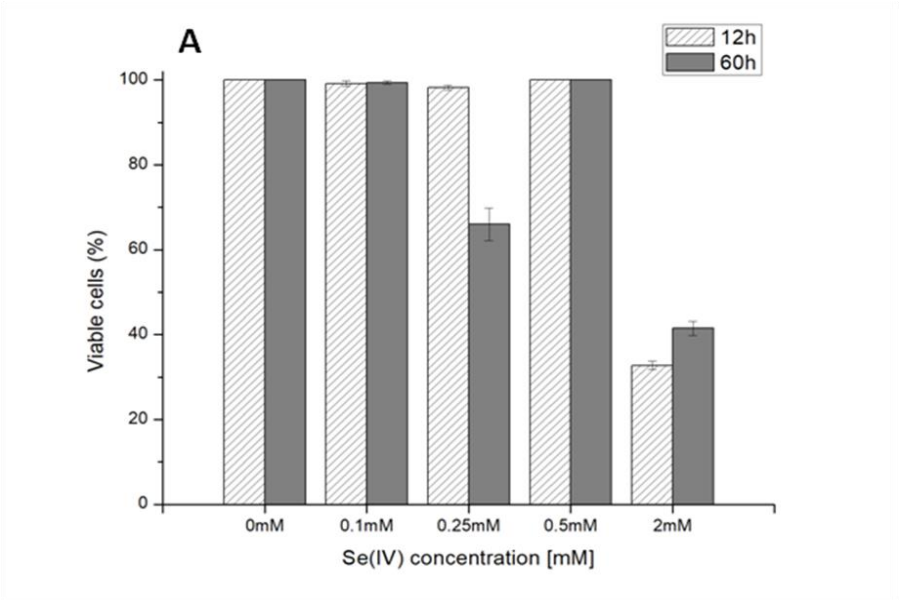

The MIND-project has received funding from the European Union's Euratom research and training program (Horizon 2020) under grant agreement 661880.

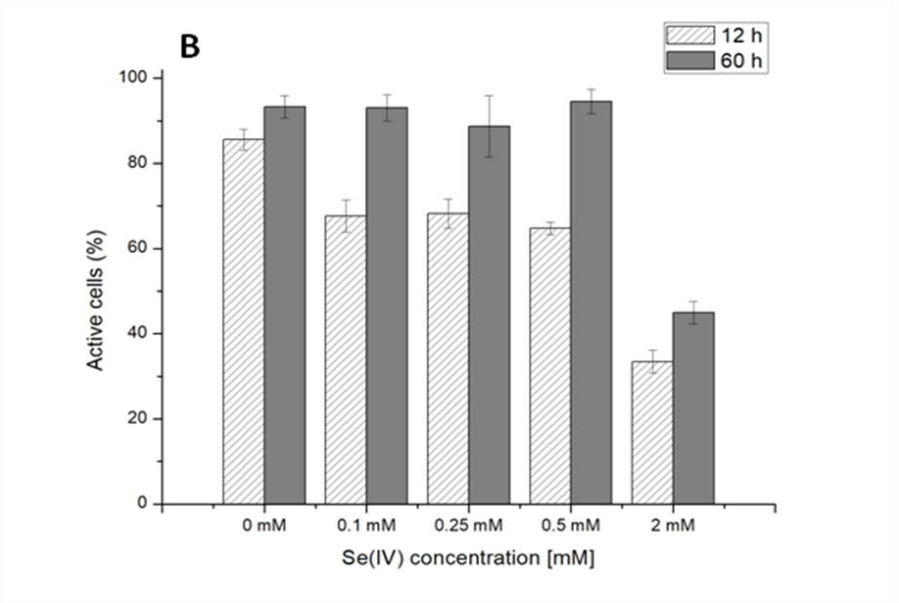

Figure 14. Percentage of viable (A) and active cells (B) of S. bentonitica under different selenite concentrations (0, 0.1, 0.25, 0.5, and 2 mM) and contact times (12 and 60 h) anaerobically.

Microscopic and spectroscopic characterization

STEM/HAADF and VPSEM micrographs showed the presence of Se nanospheres when the cells of *S. bentonitica* grown at pH 7 and 10 under anaerobic conditions during 5 days of incubation (**Figure 15A-C**). We observed a higher number of cell debris and lysed cells attached to Se nanospheres comparing with aerobic conditions (**Figure 15C**). The Raman spectrum of these nanospheres showed a peak at 252 cm^{-1} (**Figure 15D**). According to Kora *et al*. 2016 (28) the absorption peak at 254 cm^{-1} correspond to amorphous Se. However, Zhang *et al*. (29) indicated that this peak correspond to monoclinic Se. It is difficult to differentiate between amorphous and monoclinic since both contains 8-rings of Se and have the same colour (30). However, the amorphous atomic composition of Se is still under study (31).

The MIND-project has received funding from the European Union's Euratom research and training program (Horizon 2020) under grant agreement 661880.

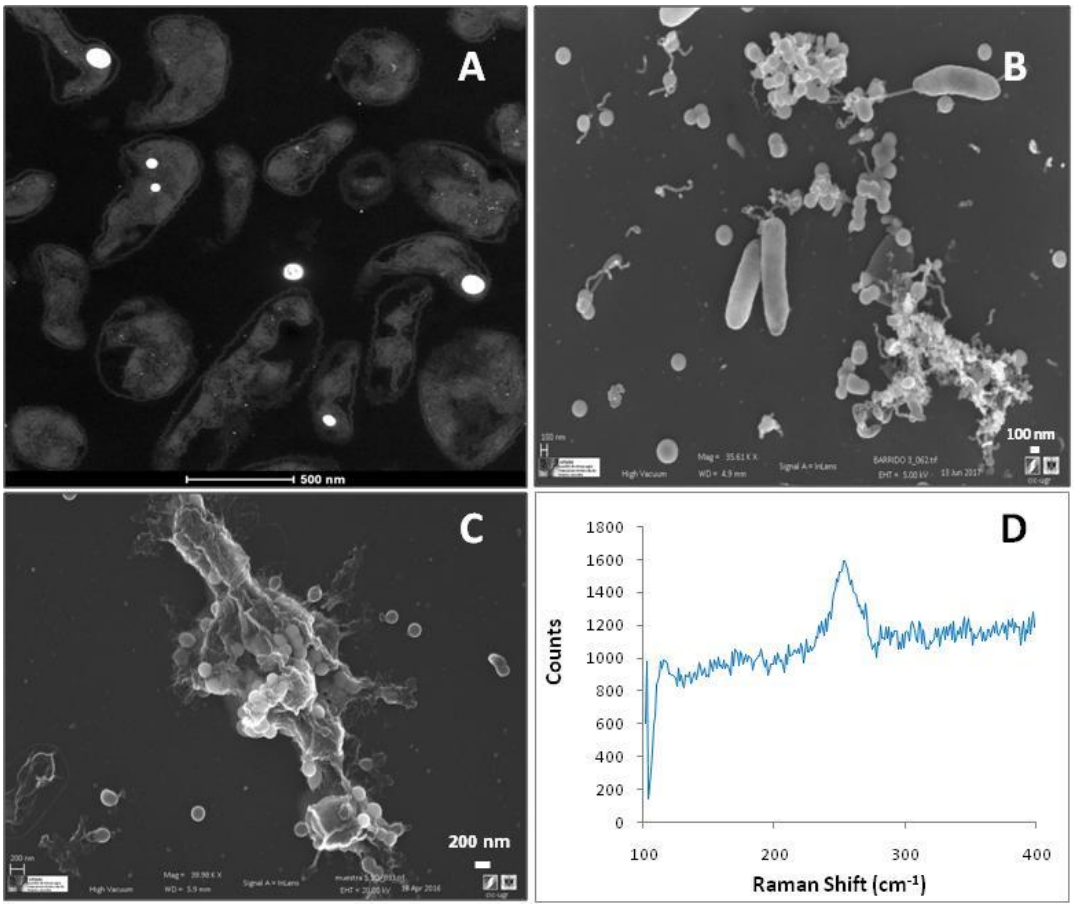

Figure 15. STEM and VP-SEM pictures showing the presence of intracellular and extracellular Se nanospheres under anaerobic and alkaline (pH 10) conditions (A, B, and C). Raman analysis derived from these nanospheres showing an absorption peak at 252 cm^{-1} (D). Scale bars: 500 nm (A), 100 nm (B) and 200 nm (C).

2.3 Se^{VI} bioreduction

Se^{VI} bioreduction and effect of Se^{VI} on the bacterial growth

The capability of *S. bentonitica* to reduce aerobically Se^{VI} to Se^{0} was tested in LB solid medium from 1 to 200 mM Se^{VI}. Bacterial cultures turned into red colour after 24h at 28°C in contrast to untreated cultures (abiotic controls and dead cells cultures supplemented with Se^{VI}) (data not shown). These results revealed that this bacterial species reduce biologically Se^{VI} to Se^{0}. Minimal inhibitory concentration of Se^{VI} was higher than 200 mM since *S. bentonitica* grew at all concentration from 1 to 200 mM, being 200 mM the maximum concentration assayed (data not shown).

The toxic effect of Se^{VI} on the bacterial growth was studied by means of total protein content as function of time (**Figure 16**). It is important to point out that microbial growth was slightly affected at 10 mM but strongly at 100 mM. Additionally, *S. bentonitica* presented longer lag phase with increasing concentrations of Se^{VI} from 10 mM to 100 mM.

The MIND-project has received funding from the European Union's Euratom research and training program (Horizon 2020) under grant agreement 661880.

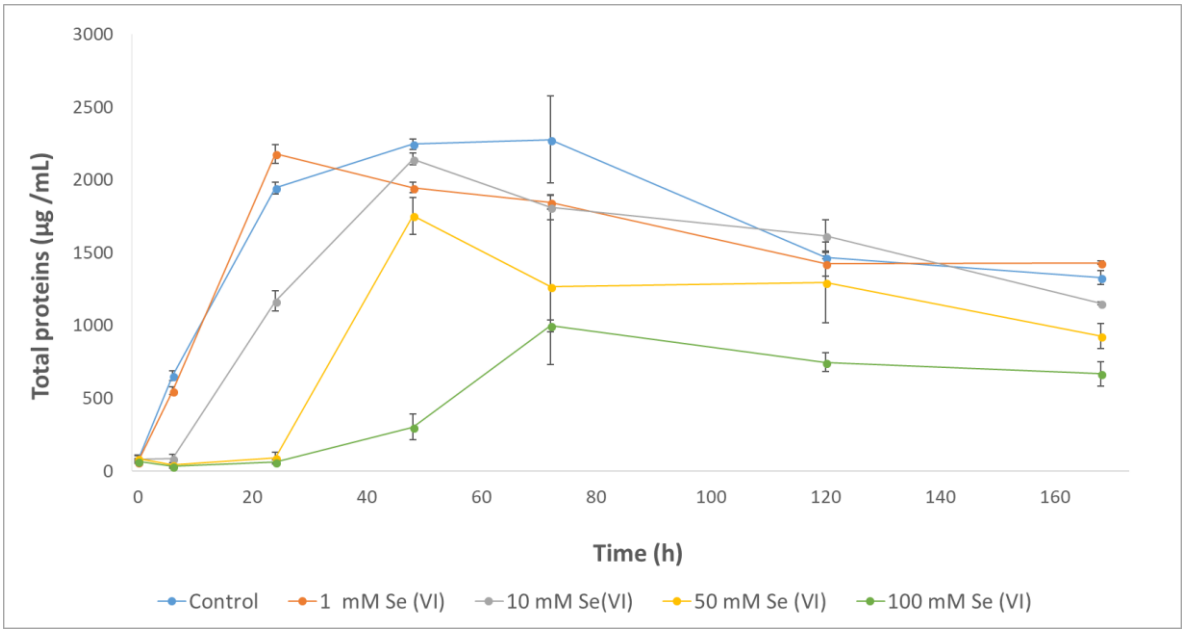

Figure 16. Effects of different selenate concentrations (0, 1, 10, 50, and 100 mM) on the growth of Stenotrophomonas bentonitica. Selenate was added at time zero. Each curve shows means based on the results of three experiments.

Structural characterization of Se reduction products

ESEM and Energy Dispersive X-ray (EDX) analysis revealed the presence of intracellular selenium structures after 24 h of incubation of *S. bentonitica* cultures amended with 200 mM Se^{VI} (**Figure 17**). Additionally, a few selenium nanowires appeared embedded in an organic matrix.

STEM micrographs and confirmed the intracellular location of selenium nanowires when cells were grown on Se^{VI} at 200 mM for 24 h (**Figure 18**). Energy Dispersive X-ray (EDX) elemental mapping derived from them revealed that they are mainly composed of Se in association with S (**Figure 18**). In addition, electron diffraction (ED) revealed their crystalline structure (data not shown).

The MIND-project has received funding from the European Union's Euratom research and training program (Horizon 2020) under grant agreement 661880.

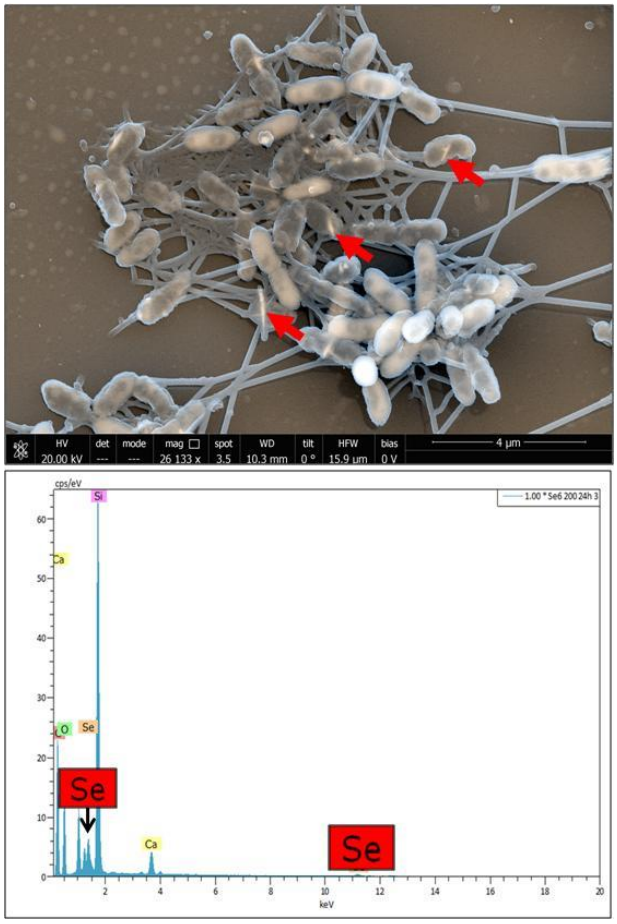

Figure 17. FEG-ESEM images showing Se nanowires located intracellularly (arrows) produced by S. bentonitica after 24 h incubation (A). EDX analysis confirming they are composed of Se (B). Scale bar: 4 µm (A).

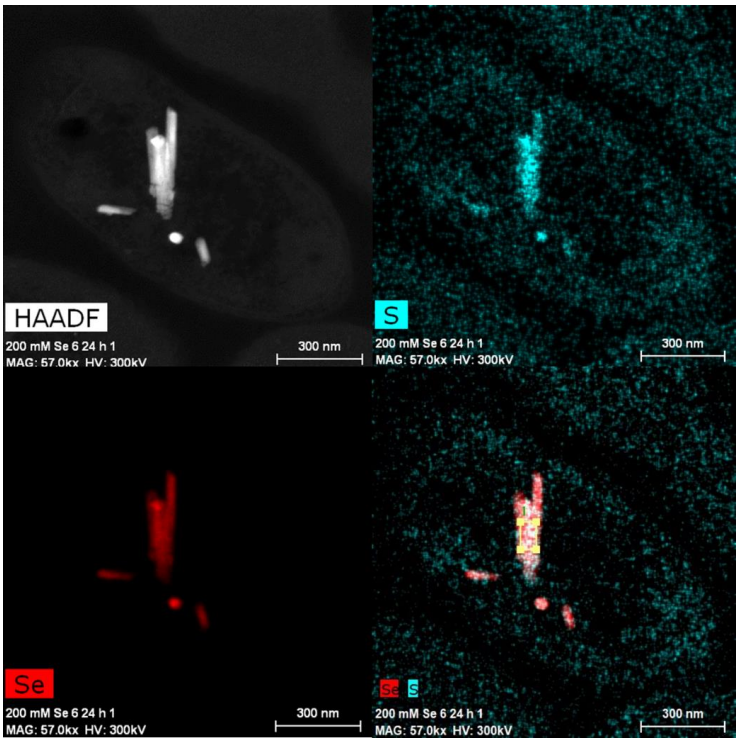

Figure 18. EDX element-distribution maps confirming the intracellular nanowires are mainly composed of Se and S. Scale bar: 300 nm.

The MIND-project has received funding from the European Union's Euratom research and training program (Horizon 2020) under grant agreement 661880.

X-ray diffraction patterns revealed the presence of elemental selenium with crystalline structure corresponding to trigonal selenium (COD-9008579) (**Figure 19**) at 2θ values of 23.59°, 29.78°, 41.47°, 43.75°,45.51°. These values correspond to crystal planes (100), (011), (110), (102), (111), respectively.

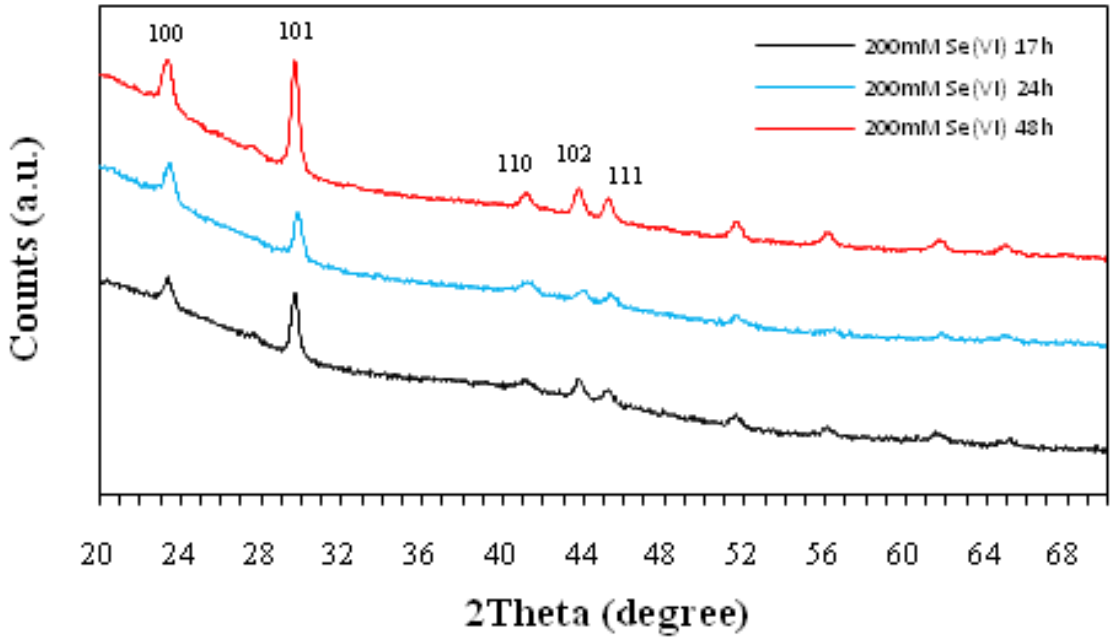

Figure 19. X-ray diffraction patterns of selenium nanoparticles produced by Stenotrophomonas bentonitica in presence of 200 mM Se^{VI} after 17, 24 and 48 h incubation.

The MIND-project has received funding from the European Union's Euratom research and training program (Horizon 2020) under grant agreement 661880.

3 The interaction of bacterial isolate *Stenotrophomonas bentonitica* from Spanish bentonites with europium

3.1 Experimental

Preparation of Europium(III) stock solution

An Europium(III) stock solution was prepared by dissolving Europium(III) chloride ($EuCl_3$) (Sigma-Aldrich) in 0.1 M HCl to a final concentration of 10 mM. For the experiments, an Europium(III) working solution was prepared diluting the stock in 0.1 M $NaClO_4$ to a final concentration of 0.03 mM. Afterwards, the pH of the solution was adjusted by addition of small volumes of acid (HCl) or base (NaOH) and sterilized by filtration through 0.22 μm nitrocellulose filters. In the case of anaerobic experiments, the solution was degassed with N_2 prior their use in a glove box.

Potentiometric Titration.

Potentiometric titrations were carried out to determine the characteristic functional groups present on the bacterial surfaces (32,33). All titrations were performed using a Metrohm Titrando 906 automatic titrator (Metrohm, UK) at 25 ºC. The temperature was kept constant and continuously monitored during the titration. The titrator was set to add successive acid or base only after a drift equal or less than 5 mV min^{-1} was achieved.

An amount of live bacteria of *S. bentonitica* equivalent to 0.4 g/L of dry biomass (washed four times with $NaClO_4$) was suspended in a vessel with 25 ml CO_2-free 0.03 mM Eu(III) solution containing 0.1 M $NaClO_4$. Bacterial samples suspended in 0.1 M $NaClO_4$ were employed as control. The suspension was titrated with 0.1 M HCl to pH 3.5 and then with 0.1 M NaOH to pH 10.0. To test the reversibility of the protonation-deprotonation behaviour, the suspension was back-titrated with 0.1 M HCl from pH 10.0 to 3.5. All the experiments were carried out in triplicate. The HCl and NaOH were previously standardized against primary standards.

To calculate the acidity constant (p*K*a) values for the bacterial cells and the corresponding total concentration of the binding sites, data from four replicates of each titration curve was fitted using the program Protofit 2.1 rev1 (34). Variations in the experimental results are reported as the average ± standard derivation. These measurements were conducted in collaboration with Prof. Jesus Ojeda, School of Engineering, University of Swansea.

Biosorption experiments

S. bentonitica cells were collected at the exponential phase of growth by centrifugation (10000 g, 10 minutes). The resultant pellet was washed three times with 0.1 M $NaClO_4$ and resuspended in it to obtain a final biomass concentration of 0.2 g/L. Then, the samples were contacted with 0.03 mM Eu(III) solution and incubated at 100 rpm on a rotator shaker at room temperature. The Eu(III)-bacteria suspension were harvested by centrifugation (10000

The MIND-project has received funding from the European Union's Euratom research and training program (Horizon 2020) under grant agreement 661880.

g, 10 minutes) after different incubation times (0, 0.5, 1, 2, 24 and 96 hours for aerobic experiments and 0, 1, 2, 18, 26 and 48 h for the anaerobic). Subsequently, 1 ml of the resultant supernatant was mixed with 1 % HNO_3 and measured by ICP-MS to estimate the Eu(III) concentration. The amount of Eu(III) adsorbed to the cells was calculated by subtracting the amount obtained in the supernatant from the initial Eu(III) concentration. For the Eu(III)-bacteria interaction under anaerobic conditions the samples were contacted with Eu(III) under nitrogen atmosphere within a glove box. Eu(III) solution (0.03 mM) without addition of cells was employed as control. All samples were performed in triplicate.

HAADF/STEM analysis

The cellular location of Eu(III) were analyzed by using Scanning-Transmission Electron Microscopy (STEM) equipped with energy dispersive X-ray (EDX) for elemental composition analysis. EDX analysis was performed at 300 kV using a spot size of 4 Å and a live counting time of 50 s. The samples consisting of Eu(III)-treated cells (0.03 mM) were prepared as described in Merroun *et al.* 2005 (12) after 48 h of incubation. Finally, the samples were examined under High-Angle Annular Dark Field Scanning Transmission Electron Microscope (HAADF-STEM) FEI TITAN G2 80-300. STEM specimen holders were cleaned by plasma prior to STEM analysis to minimize contamination.

3.2 Results

3.2.1 Potentiometric titration studies

Bacterial cell walls contain a variety of functional groups that provide metal binding sites, such as hydroxyl, phosphoryl, amino, and carboxylic groups. These functional groups can protonate or deprotonate when interacting with their immediate surroundings and as a result the cell walls develop a net pH-dependent charge (33). Therefore, knowledge of the cell surface proprieties is crucial to understand the interaction mechanisms between bacteria and surrounding metals. The potentiometric titrations curves of *S. bentonitica* BII-R7 before and after Eu(III) exposure are presented in Figures 1A and 1B.

The titrated bacterial suspensions exhibit a protonation-deprotonation behaviour over the whole pH range studied (see **Figs. 20A** and **20B**). No evidence of saturation was found with respect to proton adsorption, indicating that, even at pH 3.5, full protonation of the functional groups on the cell wall was not achieved. The shape of the titrations curves obtained suggested the presence of functional groups with close acid-base pK_a values, showing that although some small variability could be perceived in each set of the same bacterial sample, essentially reproducible results were obtained (the variation between the titration curves was below 6% of $[H^+]_{exchanged}$ between pH 3.5 and 10.0). Although a small hysteresis could be observed between acid and base titrations at the same ionic strength, results from reverse titrations did not vary strongly and suggested a reversible proton adsorption/desorption reaction.

The MIND-project has received funding from the European Union's Euratom research and training program (Horizon 2020) under grant agreement 661880.

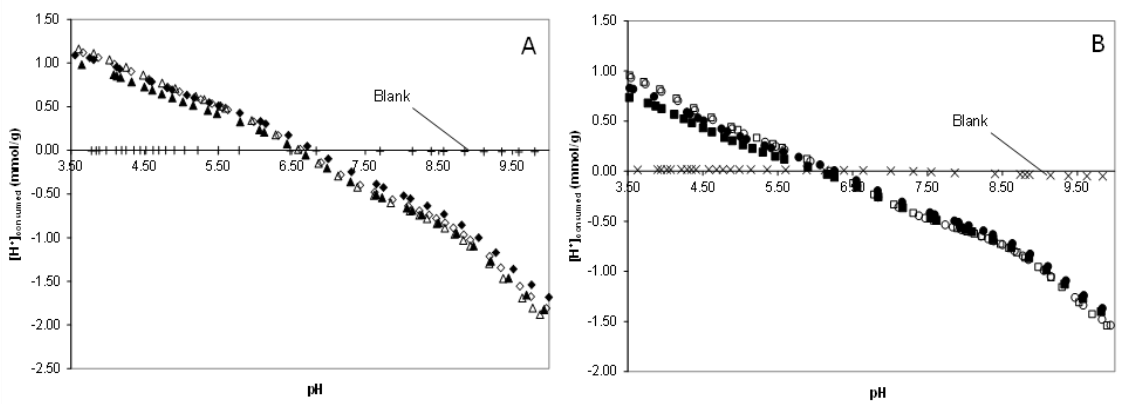

Figure 20. Representation of the potentiometric titrations of S. bentonitica BII-R7 in suspension in $NaClO_4$ (A) and in contact with Eu(III) solution (B) after 48 hours of biosorption, compared with the background electrolyte. Closed symbols correspond to the forward titration data and open symbols correspond to back titration.

The pK_a calculated values for *S. bentonitica* BII-R7 before and after Eu(III) exposure are 4.97 ± 0.08 and 4.78 ± 0.06 for pK_1 respectively, 6.88 ± 0.02 and 6.75 ± 0.13 for pK_2 and 9.43 ± 0.02 and 9.48 ± 0.11 for pK_3, respectively. The obtained pK_a values are representative of carboxylic groups for pK_1, phosphate groups for pK_2 and amine and hydroxyl groups for pK_3 (33). The existence of pH of zero proton charge (pH_{zpc}) indicated that *S. bentonitica* BII-R7 developed a positive net charge at low pH values, indicating the presence of at least one positively ionising, plausibly amino group. The pH_{zpc} around 5.7 also indicated that the cells are negatively charged at neutral pH = 7 and electrostatic attraction with positive-charged surfaces or metals may be favourable.
The surface site densities obtained using ProtoFit indicated that the pK_a values for both bacterial samples are comparable, indicating similar concentration of the active functional groups on the cell wall. However, the concentrations corresponding to phosphate groups (C_2) and amine/hydroxyl groups (C_3) are significantly lower for the BII-R7 strain exposed to Eu(III). This could suggest that the Eu(III) may be strongly bonded to phosphate and amino/hydroxyl sites, making them now inaccessible to the protonation/deprotonation reaction.

The results of potentiometric titration experiments on the studied samples indicated that the cell surface groups capable for metal binding sites involving carboxyl groups (pK around 3-5), sites involving phosphate groups (pK around 6-7), and sites involving hydroxyl and amine groups (pK > 8). These findings are in agreement with previous studies on bacterial surfaces (33,35).

3.2.2 Sorption studies at different respiring conditions.

Sorption studies of BII-R7 strain with europium (Eu) were performed in order to estimate the adsorption capacity of Eu by this bacterial strain under different respiring conditions using several contact times. These kinetic assays were performed under aerobic and anaerobic conditions in order to elucidate possible actinide-bacteria interactions under deep geological repositories conditions (Eu is an inactive analogue of trivalent actinides) by using inductively coupled plasma mass spectrometry (ICP-MS). For this purpose, the next conditions were employed: 0.2 g/L of biomass concentration, 0.03 mM Eu(III) concentration, pH 6, 0.1 M $NaClO_4$ as electrolyte and different contact times.

The MIND-project has received funding from the European Union's Euratom research and training program (Horizon 2020) under grant agreement 661880.

Results under aerobic conditions showed a maximum amount adsorbed was 129.4 Eu mg/g of dry biomass at 96 h (**Figure 21**). This amount corresponds to a 54 % of the total quantity of Eu. Regarding anaerobic experiments, the maximum value of Eu adsorbed by the cells was lower (60.6 mg Eu/g dry biomass at 18 h) (**Figure 22**), corresponding to a 31.2% of Eu adsorption. In this case, saturation was attained starting from 18 hours approximately, earlier than aerobic conditions in which saturation wasn't attained under incubation times measured. Otherwise, in both conditions the results showed an increasing of Eu adsorbed with contact time, at least in the beginning of the growth rate.

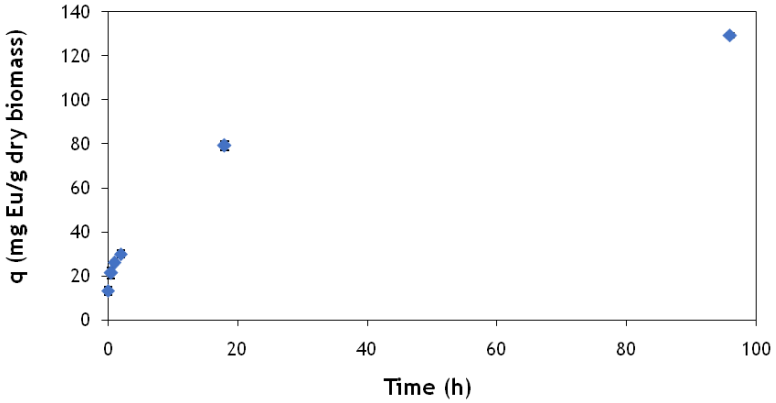

Time (h)	q (mg Eu/g dry biomass)	Eu adsorbed (%)
0	13,3 ± 1,9	5,6 ± 0,79
0,5	21,3 ± 2,4	8,9 ± 0,99
1	25,9 ± 1,1	10,8 ± 0,44
2	30 ± 1,8	12,5 ± 0,73
18	79,2 ± 2,1	33 ± 0,89
96	**129,4 ± 1,1**	**54 ± 0,44**

Figure 21. Time dependence in the amount adsorbed of Eu(III) per g of dry biomass by S. bentonitica under aerobic conditions.

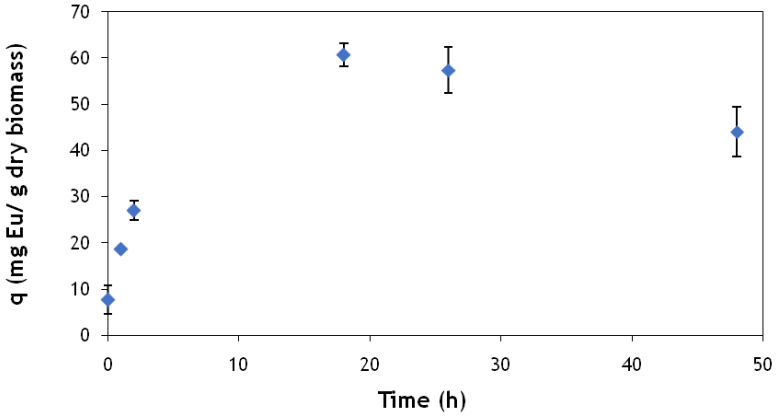

Time (h)	q (mg Eu/g dry biomass)	Eu adsorbed (%)
0	7,7 ± 3	3,9 ± 1,5
1	18,6 ± 0,3	9,6 ± 0,2
2	27 ± 2	13,9 ± 1
18	**60,6 ± 2,5**	**31,2 ± 1,3**
26	57,3 ± 4,9	29,5 ± 2,5
48	44 ± 5,3	22,6 ± 2,3

Figure 22. Time dependence in the amount adsorbed of Eu(III) per g of dry biomass by S. bentonitica under anaerobic conditions.

3.2.3 Microscopic analysis

TEM micrographs of thin sections revealed the presence of electron-dense accumulations surrounding the cell surface when cells are grown on Eu(III) after 48 h of incubation **(Figure 23A and 23B).** In a lesser proportion, intracellular and extracellular accumulations were also observed **(Figure 23A and 23B)**. EDX analysis confirmed that they are mainly composed by Eu (**Figure 23C and 23D)**. In addition, energy dispersive X-ray (EDX) elemental mapping analysis derived from these accumulates showed that they are mainly composed of Eu **(Figure 24)**. Other elements like phosphorus are also present in the Eu accumulates, suggesting the Eu-phosphorus complexation.

The MIND-project has received funding from the European Union's Euratom research and training program (Horizon 2020) under grant agreement 661880.

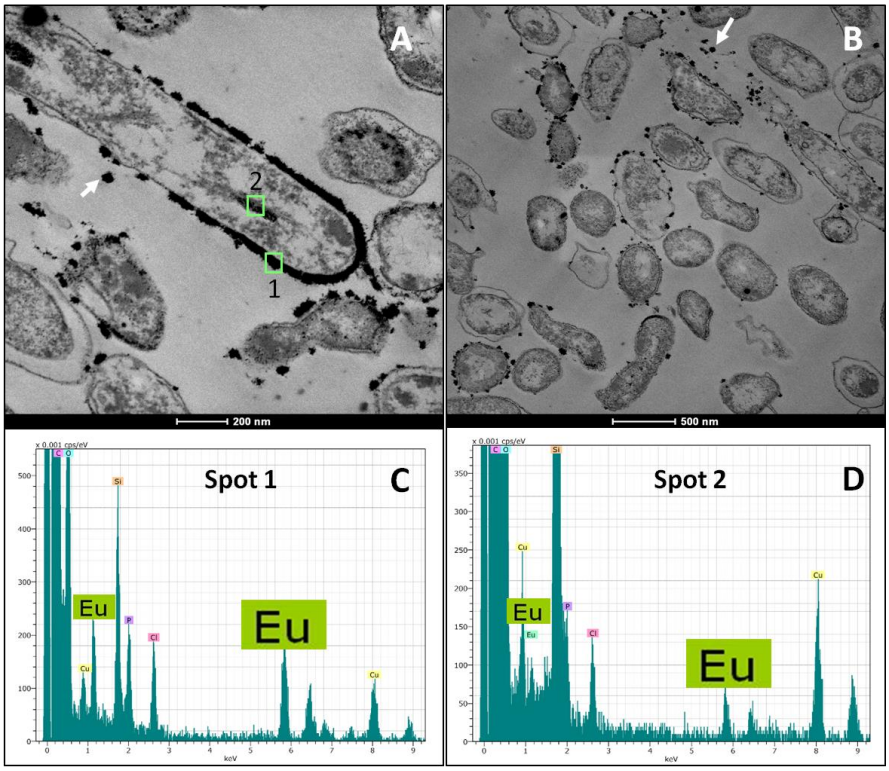

Figure 23. STEM-HAADF micrographs showing electron-dense accumulations located extracelularly (arrows), intracellularly and mainly around the cell surface (A, B). The accumulations are composed mainly of Eu(III) as determined from Energy dispersive X-ray (EDX) analysis (C and D).

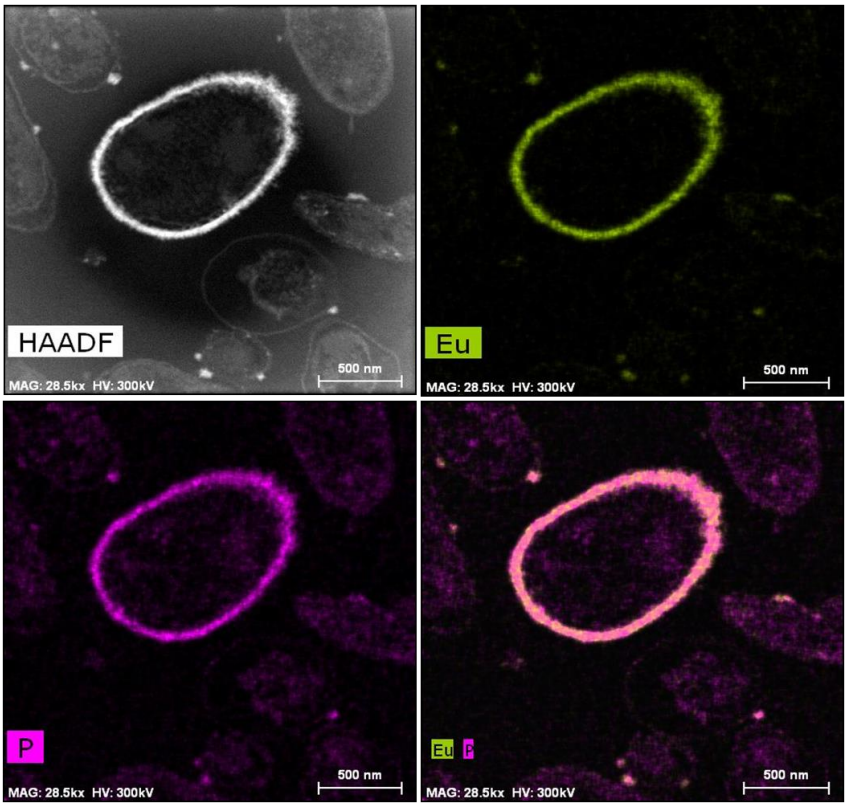

Figure 24. EDX element-distribution maps confirming that the electron-dense accumulations surrounding S. bentonitica cells are composed by Eu and P.

The MIND-project has received funding from the European Union's Euratom research and training program (Horizon 2020) under grant agreement 661880.

4 Discussion

It is well known the potential long-term exposure risk of radionuclides produced as fission and activation products from nuclear waste disposal (36). Microbes are able to interact with radionuclides through different processes affecting their transport and migration behaviour in the environment. Recent studies indicated the presence of Se in tetravalent oxidation state (Se^{IV}) in high-level nuclear wastes (37). In addition the presence of Se in hexavalent form (Se^{VI}) cannot be excluded (36). The bacteria *Stenotrophomonas bentonitica* isolated from bentonite clay formations selected for their use as buffer material around the waste canisters showed its ability to reduce Se^{VI} and Se^{IV} producing nanostructures embedded in organic matter (amorphous nanospheres and crystalline nanowires and hexagons) and volatile methylated Se forms. Many authors have reported the synthesis of SeNPs coated by organic layers mainly composed by proteins, lipids and polysaccharides (38,39). In particular, the role of proteins in the transformation of SeNPs as well as in controlling the size distribution has been previously suggested (40,41). Dobias *et al.* 2011 (41) demonstrated the role of AdhP, a single purified protein, on decreasing the average size of chemically produced SeNPs. On the other hand, Wang *et al.* 2010 (40) reported the polyvalency of proteins during the transformation from Se nanospheres to stable Se nanowires. According to them, proteins are involved in trapping on the surface and reducing the Se^{IV} ions. In addition, they suggested that proteins excreted by *Bacillus subtilis* serv as template avoiding the futher growth of monoclinic-Se and accelerating its transformation to trigonal nanowires. Although the exact mechanism of the transformation of spherical SeNPs to t-Se 1D structures in *S. bentonitica* is still unclear; the directing role of cells and their proteins is undoubtedly significant.

The bioreduction of this soluble Se species to insoluble Se forms would reduce the mobility of Se within the future DGR system. The shape of Se nanostructures is also important since it greatly affects their colloidal stability and surface charge, which in turn influences their mobility and the effectiveness of bioremediation (38). Jain *et al.* (38) demonstrated the lower colloidal stability and mobility of biogenic Se nanorods comparing with biogenic Se nanospheres produced by anaerobic granular sludge. In addition, It has been previously reported that crystallization of SeNPs increases their settleability and hence immobility through the environment (42). For this reason, the formation of Se nanowires and crystalline Se nanostructures would be beneficial for Se immobilization in future disposal of radioactive wastes. Finally, the reduction of toxic oxyanions (Se^{VI} and Se^{IV}) to volatile methylated species is considered a detoxification mechanism since methylated Se species are less toxic (43).

As an inactive analogue for trivalent actinides (e.g. Cm(III) and Am(III)) Eu has received attention to study the microbial processes involved in the immobilization of actinides. Biosorption processes consisting of ligand interaction between functional groups of microorganisms with metals is a promising technology for the bioremediation of contaminated wastes (44). The ability of *S. bentonitica* to interact with Eu(III) under both aerobic and anaerobic conditions by a biosorption process would be positive for the safety of planned nuclear repositories due to the immobilization of actinides.

The MIND-project has received funding from the European Union's Euratom research and training program (Horizon 2020) under grant agreement 661880.

5 Conclusions

This work described the reduction of toxic Se oxyanions (Se^{VI} and Se^{IV}) to less toxic species (Se^{0} and Se^{-II}) and the Eu(III) biosorption by *Stenotrophomonas bentonitica,* isolated from Spanish bentonites. This bacterial strain is able to synthesize intracellular and extracellular Se^{0} nanostructures with different shapes (spherical, hexagonal, polygonal and nanowires) and distinct crystallographic properties (amorphous and trigonal structure) when grow aerobically in presence of Se^{IV} under mesophilic conditions. For this reason we provided an environmentally friendly and economical method to fabricate biogenic Se nanostructures. Time-dependent experiments showed that the cells of *S. bentonitica* and their proteins are involved into the transformation of amorphous Se^{0} nanospheres (*a*-Se) to one-dimensional (1D) trigonal selenium (*t*-Se) nanostructures (hexagons, polygons and nanowires). However, more studies are needed to determine the exact mechanism of the transformation process. *S. bentonitica* is also able to reduce Se^{IV} under anaerobic and alkaline conditions (up to pH 10) producing a-Se nanospheres. However, the cells synthesize only intracellular Se^{0} nanowires when this strain grows aerobically in presence of Se^{VI}. The production of different volatile methylated Se species produced by *S. bentonitica* confirmed the change in the chemical speciation from Se^{VI} and Se^{IV} to Se^{-II}. On the other hand, *S. bentonitica* is able to interact with Eu(III) mainly by a biosorption process under both aerobic and anaerobic conditions.

The Se reduction and production of crystalline *t*-Se nanostructures would be of great significance within the DGR system since the mobility of Se through the surrounding environment may be reduced. The biosorption of Eu(III), as a non-radioactive analogous to An(III) characteristics of nuclear waste, would also be of importance within the DGR system due to its retention through the surrounding environment.

The potential environmental significance of this study includes understanding of the impact of microbial processes in the transport of selenium in future radioactive repositories which in turn will help to support the implementation of planned repositories.

6 Acknowledgement

The MIND-project has received funding from the European Union's Euratom research and training program (Horizon 2020) under grant agreement 661880 The MIND-project. The authors acknowledge the collaboration of Dr. Moll and Dr. Cherkouk from the HZDR (Dresden, Germany), Dr. Gardiner and Dr. Eswayah from the Sheffield Hallam University (Sheffield, UK) and Dr. Ojeda from University of Swansea (Swansea, UK) for their collaboration in the present work. In addition, the authors thank the assistance of Maria del Mar Abad Ortega, Isabel Sánchez Almazo, Isabel Guerra Tschuschke and Concepción Hernández Castillo (Centro de Instrumentación Científica, University of Granada, Spain) for their help with microscopy measurements. We also thank the assistance of José Romero Garzón and Jaime Lazuen Alcón (Centro de Instrumentación Científica, University of Granada, Spain) with the XRD and flow cytometry measurements.

The MIND-project has received funding from the European Union's Euratom research and training program (Horizon 2020) under grant agreement 661880.

7 References

1. López-Fernández M, Cherkouk A, Vilchez-Vargas R, Jauregui R, Pieper D, Boon N, et al. Bacterial Diversity in Bentonites, Engineered Barrier for Deep Geological Disposal of Radioactive Wastes. Microb Ecol. 2015;70(4):922–35.
2. Meleshyn A. Microbial Processes Relevant for Long-Term Performance of Radioactive Waste Repositories in Clays. Gesellschaftfür Anlagen-und Reaktorsicherheit (GRS) mbH, 2011. GRS – 291. ISBN 978-3-939355-67-0.
3. Merroun ML, Nedelkova M, Ojeda JJ, Reitz T, Fernández ML, Arias JM, et al. Bio-precipitation of uranium by two bacterial isolates recovered from extreme environments as estimated by potentiometric titration, TEM and X-ray absorption spectroscopic analyses. J Hazard Mater. Elsevier B.V.; 2011;197:1–10.
4. Moll H, Lütke L, Bachvarova V, Cherkouk A, Selenska-Pobell S, Bernhard G. Interactions of the Mont Terri Opalinus Clay Isolate Sporomusa sp. MT-2.99 with Curium(III) and Europium(III). Geomicrobiol J. 2014;31(8):682–96.
5. Fernandez-Llamosas H, Castro L, Blazquez ML, Diaz E, Carmona M. Biosynthesis of selenium nanoparticles by *Azoarcus* sp. CIB. Microb Cell Fact. BioMed Central; 2016;15(1):1–10.
6. Breynaert E, Scheinost AC, Dom D, Rossberg A, Vancluysen J, Gobechiya E, et al. Reduction of Se(IV) in boom clay: XAS solid phase speciation. Environ Sci Technol. 2010;44(17):6649–55.
7. Sánchez-Castro I, Bakkali M, Merroun ML. Draft genome sequence of *Stenotrophomonas bentonitica* BII-R7, a selenite-reducing bacterium isolated from Spanish bentonites. Genome Announc. 2017;5(31): e00719-17. DOI: 10.1128/genomeA.00719-17.
8. Sánchez-Castro I, Ruiz-Fresneda MA, Bakkali M, Kämpfer P, Glaeser SP, Busse HJ, et al. Stenotrophomonas bentonitica sp. nov., isolated from bentonite formations. Int J Syst Evol Microbiol. 2017;67(8):2779–86.
9. López-Fernández M, Fernández-Sanfrancisco O, Moreno-García A, Martín-Sánchez I, Sánchez-Castro I, Merroun ML. Microbial communities in bentonite formations and their interactions with uranium. Appl Geochemistry. 2014;49:77–86.
10. Dhanjal S, Cameotra SS. Aerobic biogenesis of selenium nanospheres by *Bacillus cereus* isolated from coalmine soil. Microb Cell Fact. 2010;9:52.
11. Rossbach S, Wilson TL, Kukuk ML, Carty HA. Elevated zinc induces siderophore biosynthesis genes and a zntA-like gene in Pseudomonas fluorescens. FEMS Microbiol Lett. 2000;191(1):61–70.
12. Merroun ML, Raff J, Rossberg A, Hennig C, Reich T, Selenska-Pobell S. Complexation of uranium by cells and S-layer sheets of Bacillus sphaericus JG-A12. Appl Environ Microbiol. 2005;71(9):5532–43.
13. Eswayah AS, Smith TJ, Scheinost AC, Hondow N, Gardiner PHE. Microbial transformations of selenite by methane-oxidizing bacteria. Appl Microbiol Biotechnol. Applied Microbiology and Biotechnology; 2017;101(17):6713–24.
14. Sabaty M, Avazeri C, Pignol D, Vermeglio A. Characterization of the Reduction of Selenate and Tellurite by Nitrate Reductases. Appl Environ Microbiol. 2001;67(3–12):5122–6.
15. Vogel M, Fischer S, Maffert A, Hübner R, Scheinost AC, Franzen C, et al. Biotransformation and detoxification of selenite by microbial biogenesis of selenium-sulfur nanoparticles. J Hazard Mater. 2018;344:749–57.

The MIND-project has received funding from the European Union's Euratom research and training program (Horizon 2020) under grant agreement 661880.

16. Hunter WJ. A rhizobium selenitireducens protein showing selenite reductase activity. Curr Microbiol. 2014;68(3):311–6.

17. Kessi J, Hanselmann KW. Similarities between the abiotic reduction of selenite with glutathione and the dissimilatory reaction mediated by Rhodospirillum rubrum and Escherichia coli. J Biol Chem. 2004;279(49):50662–9.

18. Yamada A, Miyashita M, Inoue K, Matsunaga T. Extracellular reduction of selenite by a novel marine photosynthetic bacterium. Appl Microbiol Biotechnol. 1997;48(3):367–72.

19. Zawadzka AM, Crawford RL, Paszczynski AJ. Pyridine-2,6-bis(thiocarboxylic acid) produced by Pseudomonas stutzeri KC reduces and precipitates selenium and tellurium oxyanions. Appl Environ Microbiol. 2006;72(5):3119–29.

20. Basaglia M, Toffanin A, Baldan E, Bottegal M, Shapleigh JP, Casella S. Selenite-reducing capacity of the copper-containing nitrite reductase of Rhizobium sullae. FEMS Microbiol Lett. 2007;269(1):124–30.

21. Givan AL. Flow Cytometry: An Introduction. In: Hawley TS, Hawley RG (eds.) Flow Cytometry Protocols, 3rd Ed. Humana Press (Springer Science+Business Media), New York. 2011; 1-30.

22. Stubberfield LCF, Shaw PJA. A comparison of tetrazolium reduction and FDA hydrolysis with other measures of microbial activity. J Microbiol Methods. 1990;12(3–4):151–62.

23. David F, Berger A, Hänsch R, Rohde M, Franco-Lara E. Single cell analysis applied to antibody fragment production with Bacillus megaterium: Development of advanced physiology and bioprocess state estimation tools. Microb Cell Fact. 2011;10.

24. Ruiz-Fresneda MA, Delgado-Martin J, Gomez-Bolivar J, Fernandez-Cantos MV, Bosch-Estevez G, Martinez-Moreno MF, Merroun ML. Environmental Science : Nano (in press).

25. Gates B, Mayers B, Cattle B, Xia Y. Synthesis and characterization of uniform nanowires of trigonal selenium. Adv Funct Mater. 2002;12(3):219–27.

26. Wang T, Yang L, Zhang B, Liu J. Extracellular biosynthesis and transformation of selenium nanoparticles and application in H2O2 biosensor. Colloids Surfaces B Biointerfaces. 2010;80(1):94–102.

27. Chasteen TG. Confusion between dimethyl selenenyl sulfide and dimethyl selenone released by bacteria. Appl Organomet Chem. 1993;7(5):335–42.

28. Kora AJ, Rastogi L. Bacteriogenic synthesis of selenium nanoparticles by Escherichia coli ATCC 35218 and its structural characterisation. 2016;179–84.

29. Zhang W, Chen Z, Liu H, Zhang L, Gao P, Li D. Biosynthesis and structural characteristics of selenium nanoparticles by Pseudomonas alcaliphila. Colloids Surfaces B Biointerfaces. Elsevier B.V.; 2011;88(1):196–201.

30. Minaev VS, Timoshenkov SP, Kalugin V V. Structural and phase transformations in condensed selenium. J Optoelectron Adv Mater. 2005;7(4):1717–41.

31. Fernández-Martínez A, Charlet L. Selenium environmental cycling and bioavailability: a structural chemist point of view. Rev Environ Sci Bio/Technology. 2009 Feb 7 [cited 2015 Jan 7];8(1):81–110.

32. Fein JB, Boily JF, Yee N, Gorman-Lewis D, Turner BF. Potentiometric titrations of Bacillus subtilis cells to low pH and a comparison of modeling approaches. Geochim Cosmochim Acta. 2005;69(5):1123–32.

33. Ojeda JJ, Romero-González ME, Bachmann RT, Edyvean RGJ, Banwart SA. Characterization of the cell surface and cell wall chemistry of drinking water bacteria by combining XPS, FTIR

The MIND-project has received funding from the European Union's Euratom research and training program (Horizon 2020) under grant agreement 661880.

spectroscopy, modeling, and potentiometric titrations. Langmuir. 2008;24(8):4032–40.

34. Turner BF, Fein JB. Protofit: A program for determining surface protonation constants from titration data. Comput Geosci. 2006;32(9):1344–56.

35. Haas JR, Dichristina TJ, Wade R. Thermodynamics of U(VI) sorption onto Shewanella putrefaciens. Chem Geol. 2001;180(1–4):33–54.

36. Grambow B. Mobile fission and activation products in nuclear waste disposal. J Contam Hydrol. 2008;102(3–4):180–6.

37. Dardenne K, González-Robles E, Rothe J, Müller N, Christill G, Lemmer D, et al. XAS and XRF investigation of an actual HAWC glass fragment obtained from the Karlsruhe vitrification plant (VEK). J Nucl Mater. 2015;460:209–15.

38. Jain R, Jordan N, Tsushima S, Hübner R, Weiss S, Lens PNL. Shape change of biogenic elemental selenium nanomaterials from nanospheres to nanorods decreases their colloidal stability. Environ Sci Nano. Royal Society of Chemistry; 2017;4(5):1054–63.

39. Kamnev AA, Mamchenkova P V., Dyatlova YA, Tugarova A V. FTIR spectroscopic studies of selenite reduction by cells of the rhizobacterium Azospirillum brasilense Sp7 and the formation of selenium nanoparticles. J Mol Struct. 2017;1140:106–12.

40. Wang T, Yang L, Zhang B, Liu J. Extracellular biosynthesis and transformation of selenium nanoparticles and application in H2O2biosensor. Colloids Surfaces B Biointerfaces. 2010;80(1):94–102.

41. Dobias J, Suvorova EI, Bernier-Latmani R. Role of proteins in controlling selenium nanoparticle size. Nanotechnology. 2011;22(19).

42. Lenz M, van Aelst AC, Smit M, Corvini PFX, Lens PNL. Biological production of selenium nanoparticles from waste waters. Adv Mater Res. 2009;71–73:721–4.

43. Frankenberger WT, Arshad M. Bioremediation of selenium-contaminated sediments and water. BioFactors. 2001;14(1–4):241–54.

44. Francis AJ. Biotransformation of uranium and other actinides in radioactive wastes. J Alloys Compd. 1998;271–273:78–84.

The MIND-project has received funding from the European Union's Euratom research and training program (Horizon 2020) under grant agreement 661880.